Fatigue And Fracture Of Cylindrical Shells With A Circumferential Crack.

FATIGUE AND FRACTURE OF CYLINDRICAL SHELLS WITH A CIRCUMFERENTIAL CRACK

by

Mohan M. Ratwani

A Dissertation

Presented to the Graduate Committee

of Lehigh University

in candidacy for the Degree of

Doctor of Philosophy

in

Engineering Mechanics

Lehigh University

1970

Approved and recommended for acceptance as a dissertation in partial fulfillment of the requirements for the degree of Doctor of Philosophy.

Aug 28, 1970
(date)

Fazil Erdogan
Dr. Fazil Erdogan
Professor in Charge

Accepted Sept. 8, 1970
(date)

Special committee directing the doctoral work of Mr. Mohan M. Ratwani

Richard Roberts
Prof. Richard Roberts
Chairman

Fazil Erdogan
Prof. Fazil Erdogan

R. P. Wei
Prof. R. P. Wei

R. Folk
Prof. R. Folk

Dean P. Updike
Prof. Dean Updike

ACKNOWLEDGEMENTS

The author wishes to express his deep gratitude to Prof. Fazil Erdogan for his immeasurable patience and guidance throughout this work.

Special thanks go to Prof. R. P. Wei and Prof. Richard Roberts for their suggestions in experimental work.

Thanks go to Dr. Dean Updike for his useful suggestions in plasticity problem in shells and to Prof. R. Folk for his suggestions in certain mathematical aspects.

This work was supported by National Aeronautics and Space Administration.

TABLE OF CONTENTS

LIST OF FIGURES

LIST OF TABLES

NOMENCLATURE

a	Half crack length
a_c	Half critical crack length
a_o	Half initial crack length
a_p	Half crack length considering plastic zone
B_m , B_b	Stress intensity factor ratios in symmetric problem
C_m , C_b	Stress intensity factor ratios in anti-symmetric problem
C	Empirical constant in fatigue model
D	Flexural rigidity
E	Young's modulus
F	Stress function
G	Shear modulus
$\mathcal{G}$	Crack extension force
h	Shell thickness
h_{ij}	Kernels in anti-symmetric problem
i	$\sqrt{-1}$
K	Stress intensity factor as defined in text
k_p	Stress intensity factor for plate
K_c	Critical plane stress, stress intensity factor at fracture
K_T	Threshhold value of stress intensity factor
K_{ij}	Fredholm kernels in anti-symmetric problem
L_{ij}	Kernels in symmetric problem

M_x , M_y , M_{xy}	Bending moment components
N_x , N_y , N_{xy}	Membrane forces
N_o , M_o , V_o , τ_o	Residual stresses along crack
p	Size of plastic zone ahead of a crack tip
q	Surface traction
Q_x , Q_y	Transverse shear forces
R	Shell radius
R_{ij}	Fredholm kernels in symmetric problem
r	Polar coordinate
SE	Log mean square standard error
T_k	Chebischev polynomials
U_n	Chebischev polynomials
u	Crack opening displacement
$u_1(t)$, $u_2(t)$	Functions in anti-symmetric problem
$u_1(0,\alpha)$, $u_2(0,\alpha)$	Crack opening displacement
w	Displacement function
X,Y,Z	Rectangular coordinates
x,y,z	Dimensionless coordinates
α	Constant as defined in text
δ	Crack opening displacement
ν	Poisson's ratio
λ	Shell parameter defined by $[12(1-\nu^2)]^{1/4} a/\sqrt{Rh}$

λ_b	Shell parameter defined by $[12(1-\nu^2)]^{1/4} a_b/\sqrt{Rh}$
φ_1, φ_2	Functions in symmetric problem
θ	Polar coordinates
σ_y	Yield strength
$\sigma_x^\infty, \sigma_y^\infty$	Stresses applied at infinity
$\sigma_{xx}^m, \sigma_{yy}^m, \tau_{xy}^m$	Extensional shell stresses
$\sigma_{xx}^b, \sigma_{yy}^b, \tau_{xy}^b$	Bending shell stresses
ε_x	Strain in x-direction

ABSTRACT

The symmetric and anti-symmetric problems of cylindrical shells with a circumferential crack are considered. For a uniform stress away from the crack the membrane and bending components of stress intensity factors are obtained within the confines of an eighth order linear shallow shell theory.

The plastic deformations and the crack opening displacement are also considered. The plastic strip model is used to calculate the plastic zone size. The crack opening displacement is calculated as the crack surface displacement at the crack tips by using the superposition technique.

Crack propagation data are collected by subjecting 6061-T4 aluminum cylinders to axial fatigue. Using two different empirical models the shell data are analyzed along with plate data.

The effect of environment on crack propagation in plates and shells is studied. Comparison is made of fatigue crack propagation rates in plates and shells in distilled water, dry atmospheric conditions and normal environments prevailing in the laboratory.

It is shown that the theoretically computed stress

intensity factors can be used to predict fatigue crack propagation behavior of shells from that of plates with same material and thickness.

Experimental results show that there is no significant difference in crack propagation rates in distilled water and normal atmospheric conditions in the laboratory but, however, there is considerable difference in crack propagation rates in distilled water and dry conditions.

I. INTRODUCTION

The study of fatigue crack propagation in shell like structures has attracted considerable interest in recent years because of its considerable importance in the design of aerospace and hydrospace structures. The crack is generally nucleated quite early in the fatigue life of the structure and the major portion of the total life of the structure is devoted to fatigue crack propagation. Hence the study of fatigue crack propagation becomes necessary in order to establish the useful life of the shell-like structures.

In the present investigation the fatigue crack propagation and fracture properties of cylindrical shells with circumferential cracks are studied theoretically and experimentally. The purpose of this study was to compute theoretically stress intensity factors in cylindrical shells with a circumferential crack under symmetric and anti-symmetric loading conditions, to develop a model for the plastic zone size and crack opening displacement ahead of the crack tip and to determine if the behavior of a crack or a crack like flaw in a shell can be predicted from the known behavior of a similar flaw in a flat plate of the same material, thickness and subjected to similar loading and atmospheric conditions.

Approximate solutions of the governing differential equations with appropriate boundary conditions for cylindrical and spherical shells containing straight through cracks have been presented by several authors [1-6]. References [1-3] give the asymptotic solutions for internally pressurized cracked spherical shell, cylindrical shell with an axial crack and cylindrical shell with a circumferential crack. These solutions are valid for small values of the shell parameter (i.e. for $\lambda < 1$) for which the deviation from a flat plate solution is not very significant. More complete solutions of the problem (i.e. for λ up to 8) are given in [4] and [6]. In [5] the effect of a circumferential stiffener in a cylindrical shell with an axial crack is studied. For the case of a cylindrical shell with a circumferential crack the only solution available is the asymptotic solution for symmetric loading given by Folias [3]. In all these studies it is assumed that the shell is "symmetrically loaded". More precisely, the solutions are based on the assumption that the unknown functions F, the stress function, and w, the out-of-plane displacement are even functions of the independent variable X and Y measured along the (projected) orthogonal axes. Folias attempted the anti-symmetric problem of spherical shell with a meridional crack, however, he could not get the solution as he did not define the unknown functions in the integral

equations properly with the result that the kernels in the integral equations had higher order singularities and the solution to the integral equations could not be obtained.

The linear fracture mechanics has established itself as a very satisfactory theoretical working tool in studying the phenomenon of fatigue crack propagation and brittle fracture in structural solids. The theories of failure or the failure criteria based on the use of the stress intensity factor, K, or the crack extension force, $\mathcal{G}$, have been most effective in cases for which the size of plastic zone ahead of the crack tip is small. Thus, these theories can be applied very effectively to plane strain fracture and high cycle fatigue crack propagation. However, in the presence of moderately large plastic deformations, the models need some re-interpretation or modification. Generally the model is modified by either assuming an increased crack length (usually by adding the plastic zone size to the crack length) for the purpose of evaluating K or $\mathcal{G}$ [7] or by introducing the concept of "crack opening displacement" [8]. The plastic zone size to be used in the first method may be obtained by using the plastic strip model introduced by Dugdale [9] (see also, [10] and [11]). Justification for the wide spread use of this modification lies not in the soundness of the underlying

physical arguments but primarily in the fact that, in most cases involving the fracture of materials with high toughness, it seems to work.

The most widely accepted definition of the crack opening displacement is the relative displacement between the opposing surfaces of the crack at the location corresponding to the actual crack tip obtained from the solution in which the leading edge of the crack is assumed to be at the elastic-plastic boundary. In Irwin's analysis this corresponds to the relative crack surface displacement at a distance r_y from the crack tip, r_y being the estimate of the plastic zone size. In [11-13] the crack opening displacement was assumed to be the relative crack surface displacement at the (actual) crack tip obtained from the solution based on the plastic strip model. The differences between the results obtained by using various modifications of the original model mentioned above are insignificant if the plastic zone size is relatively small compared to the crack length. However, they become increasingly more significant as the relative size of the plastic zone becomes larger. At present, even though far from being perfect, these models seem to be the only satisfactory theoretical tools available and are being widely used.

In view of above considerations, it was proposed to carry out the following investigations:

(a) obtain the solution for stress intensity factors for a circumferential crack in a cylindrical shell under axial tension for a wider range of shell parameters and crack lengths.

(b) obtain the solution for stress intensity factors for a circumferential crack in a cylindrical shell under torsion.

(c) to develop a model for the plastic zone size ahead of the crack tip in a cylindrical shell with a circumferential crack, using the concept of Dugdale's model.

(d) calculate the crack opening displacement.

(e) determine if the fatigue and fracture properties of cracked shells can be simply predicted from the corresponding properties of flat plates.

(f) compare fatigue crack propagation rates in plates and shells under controlled and laboratory environments.

II. ELASTIC SOLUTION FOR CYLINDRICAL SHELL WITH A CIRCUMFERENTIAL CRACK--SYMMETRIC AND ANTI-SYMMETRIC PROBLEMS

In this chapter the solution for the stress singularities at the ends of a circumferential crack in thin cylindrical shell is briefly outlined. The problem is solved within the confines of an eighth order linearized shallow shell theory, i.e. under the Kirchoff type assumption regarding the boundary conditions. The solution is applicable to linear-elastic, homogeneous and isotropic shells of constant thickness. The deformations are assumed to be small so that Hooke's law may be applied to relate stresses and strains in the shells.

2.1 Anti-Symmetric Problem

2.11 Formulation of the problem.

The following equations due to Marguerre [14] are used to formulate the problem.

$$\frac{E h a^2}{R} \frac{\partial^2 \omega}{\partial x^2} + \nabla^4 F = 0$$

$$\nabla^4 \omega - \frac{a^2}{RD} \frac{\partial^2 F}{\partial x^2} = \frac{q a^4}{D} \qquad (2.1)$$

$$x = \frac{x}{a} \quad , \quad y = \frac{Y}{a} \quad , \quad D = \frac{E h^3}{12(1-\nu^2)}$$

where F is the stress function, w is the normal displacement, q is the normal traction, E and ν are the elastic constants, and the coordinates X, Y and the dimensions a, h, R are shown in Figure 1. The stress resultants N_{ij}, the moment resultants M_{ij}, the components of transverse shear Q_j and the effective transverse shear V_x are given in terms of F and w as

$$N_{xx} = \frac{1}{a^2} \frac{\partial^2 F}{\partial y^2}$$

$$N_{yy} = \frac{1}{a^2} \frac{\partial^2 F}{\partial x^2}$$

$$N_{xy} = -\frac{1}{a^2} \frac{\partial^2 F}{\partial x \partial y} \qquad (2.2)$$

$$M_{xx} = -\frac{D}{a^2} \left[\frac{\partial^2 w}{\partial x^2} + \nu \frac{\partial^2 w}{\partial y^2} \right]$$

$$M_{yy} = -\frac{D}{a^2} \left[\frac{\partial^2 w}{\partial y^2} + \nu \frac{\partial^2 w}{\partial x^2} \right]$$

$$M_{xy} = -\frac{D}{a^2} (1-\nu^2) \frac{\partial^2 w}{\partial x \partial y}$$

$$V_x = -\frac{D}{a^3} \left[\frac{\partial^3 w}{\partial x^3} + (2-\nu) \frac{\partial^3 w}{\partial x \partial y^2} \right]$$

$$Q_x = -\frac{D}{a^3} \frac{\partial}{\partial x} (\nabla^2 w)$$

$$Q_y = -\frac{D}{a^3} \frac{\partial}{\partial y} (\nabla^2 w) \qquad (2.3)$$

The extensional components of the shell stresses are given by

$$\sigma_{xx}^{m} = \frac{1}{a^2 h} \frac{\partial^2 F}{\partial y^2}$$

$$\sigma_{yy}^{m} = \frac{1}{a^2 h} \frac{\partial^2 F}{\partial x^2}$$

$$\sigma_{xy}^{m} = -\frac{1}{a^2 h} \frac{\partial^2 F}{\partial x \partial y} \qquad (2.4)$$

and the bending stress components are given by

$$\sigma_{xx}^{b} = -\frac{EZ}{1-\nu^2} \left[\frac{\partial^2 W}{\partial x^2} + \nu \frac{\partial^2 W}{\partial y^2} \right]$$

$$\sigma_{yy}^{b} = -\frac{EZ}{1-\nu^2} \left[\frac{\partial^2 W}{\partial y^2} + \nu \frac{\partial^2 W}{\partial x^2} \right]$$

$$\sigma_{xy}^{b} = -2GZ \frac{\partial^2 W}{\partial x \partial y} \qquad (2.5)$$

The anti-symmetric problem is considered in details here. In the solution it is assumed that the only external loads

acting on the shell are the (statically self-equilibrating) tractions applied on the crack surface which are given by

$$\left.\begin{aligned} N_{xx} &= 0 \\ M_{xx} &= 0 \end{aligned}\right\} \qquad x = 0 \qquad |y| \geq 0 \tag{2.6}$$

$$N_{xy} = -\frac{1}{a^2}\frac{\partial^2 F}{\partial x \partial y} = -N^{\circ}_{xy}(y)$$

$$V_x = -\frac{D}{a^3}\left[\frac{\partial^3 w}{\partial x^3} + (2-\nu)\frac{\partial^3 w}{\partial x \partial y^2}\right] = -V_{\circ}(y)$$

$$x = 0 \qquad |y| < 1 \tag{2.7}$$

By properly combining this solution with that of an uncracked shell, the solution for a cracked shell under arbitrary anti-symmetric loads can be obtained.

In (2.6) $N_{xx} = 0$ and $M_{xx} = 0$ for $|y| \geq 1$ as well as $|y| < 1$ because of assumed symmetry.

Using Fourier transforms, the solution of the system of differential equations (2.1) satisfying the proper symmetry conditions at infinity may be expressed as follows:

$$w(x,y) = \operatorname{sgn}(x) \int_0^\infty \left[P_1 e^{(\alpha_1 - s_1)|x|} + P_2 e^{-(\alpha_1 + s_1)|x|} + P_3 e^{-(\alpha_2 + s_2)|x|} + P_4 e^{(\alpha_2 - s_2)|x|} \right] \sin(sy)\, ds$$

$$F(x,y) = \frac{i E h a^2}{R} \operatorname{Sgn}(x) \int_0^\infty \left[P_1 e^{(\alpha_1 - s_1)|x|} + P_2 e^{-(\alpha_1 + s_1)|x|} - P_3 e^{-(\alpha_2 + s_2)|x|} - P_4 e^{-(\alpha_2 - s_2)|x|} \right] \sin(sy)\, ds \qquad (2.8)$$

where

$$s_1 = (s^2 + \alpha_1^2)^{\frac{1}{2}} \qquad s_2 = (s^2 + \alpha_2^2)^{\frac{1}{2}}$$

$$\alpha_1 = \frac{\lambda}{2} e^{i\pi/4}, \quad \alpha_2 = \frac{\lambda}{2} e^{-i\pi/4}, \quad \lambda = \left(\frac{E h a^4}{R^2 D} \right)^{1/4}$$

and $P_j(s)$ are unknown. The condition $N_x(o,y) = 0$ and $M_x(o,y) = 0$ for $|y| \geq 0$ give

$$P_1 + P_2 = P_3 + P_4$$

$$P_3 - P_4 = \frac{i s_1}{s_2} (P_1 - P_2) - 2(1-\nu) \frac{s^2}{\alpha_2 s_2} (P_1 + P_2) \qquad (2.9)$$

Two more relations for P_j are obtained in the form of a system of integral equations by using the boundary conditions (2.7) at x=0. Thus for $|y|<1$ substituting from (2.7) into (2.8) and using (2.9) one finds

$$\lim_{|x|\to 0} \int_0^\infty \left[\alpha_1 (P_1 - P_2)\left(e^{-s_1|x|} + \frac{s_1}{s_2} e^{-s_2|x|}\right) + (P_1+P_2)\right.$$

$$\left.\left\{ - s_1 e^{-s_1|x|} + s_2 e^{-s_2|x|} - (1-\nu)\frac{s^2}{s_2} e^{-s_2|x|}\right\}\right]$$

$$s \cos(ys)\, ds = \frac{\lambda^2 R}{2Eh} N^\circ_{xy}(y)$$

$$|y| < 1 \qquad (2.10)$$

$$\lim_{|x|\to 0} \int_0^\infty \left[(P_1 - P_2)\left\{ e^{-s_1|x|}\left(4\alpha_1^3 + (1+\nu)\alpha_1 s^2\right) - e^{-s_2|x|}\right.\right.$$

$$\left.\left(4\alpha_2^2 \alpha_1 \frac{s_1}{s_2} + (1+\nu)\alpha_1 \frac{s_1}{s_2} s^2\right)\right\} + (P_1+P_2)\left\{ e^{-s_1|x|}\right.$$

$$\left.\left(-4\alpha_1^2 s_1 + (1-\nu) s^2 s_1\right) + e^{-s_2|x|}\left(-4\alpha_2^2 s_2 + \right.\right.$$

$$\left.\left.(1-\nu) s^2 (s_2 + 4\alpha_2^2/s_2) + (1-\nu^2) s^4/s_2\right)\right\}\Big]$$

$$(1-\cos(sy))\frac{ds}{s} = \frac{\alpha^3}{D}\int_0^y V_x^\circ(y)\, dy \qquad (2.11)$$

$$|y| < 1$$

where for dimensional consistency equation (2.11) has been integrated in y. Also, in order to separate the divergent parts of the kernels in the analysis that follows, $e^{-c_j|x|}$ terms have been retained under the integral sign.

Outside the cut, all the physical quantities and their first derivatives must be continuous. To fulfill these conditions, it is sufficient to have

$$\frac{\partial^n}{\partial x^n}\begin{pmatrix} F \\ w \end{pmatrix}^+ = \frac{\partial^n}{\partial x^n}\begin{pmatrix} F \\ w \end{pmatrix}^- ,$$

$$(n = 0,1,2,3)$$

$$|y| > 1 \ , \quad x = 0 \qquad (2.12)$$

where the superscripts + and - refer to the values of the function as x approaches zero from + and - side, respectively. Analytically this simply requires that the functions which are odd in x must vanish for x=0, $|y| > 1$. It can be easily shown that conditions (2.12) are satisfied if the functions $P_j(s)$ satisfy the following conditions:

$$\int_0^\infty (P_1 + P_2) \ \sin(sy)\, ds = 0 \qquad |y| > 1 \qquad (2.13)$$

$$\int_0^\infty (P_1 + P_2) \ s^2 \sin(sy)\, ds = 0 \qquad |y| > 1 \qquad (2.14)$$

$$\int_0^\infty \alpha_1 s_1 (P_1 - P_2) \sin(sy)\, ds = 0 \qquad |y| > 1$$

(2.15)

Here (2.13) is the condition $w=0$ at $x=0$, $|y|>1$.

Since (2.14) follows from (2.13), (2.13-2.15) are equivalent to only two conditions, which, together with (2.10) and (2.11) give a system of dual integral equations to determine P_1 and P_2.

To solve the system of dual integral equations (2.10), (2.11), (2.13) and (2.15) the following auxiliary functions are first defined:

$$\int_0^\infty \alpha_1 s_1 (P_1 - P_2) \sin(st)\, ds = u_1(t) \tag{2.16}$$

$$\int_0^\infty s^2 (P_1 + P_2) \sin(st)\, ds = u_2(t) \tag{2.17}$$

where by (2.14) and (2.15), $u_1(t)=0$ and $u_2(t)=0$ for $|t|>1$. u_1 and u_2 are defined in terms of (2.14) and (2.15) rather than (2.13) and (2.15) for dimensional consistency. Condition (2.13) on w has not yet been satisfied. This

condition is used to determine the arbitrary constants arising from the solution of the integral equations. u_1 and u_2 are related to the second derivatives of F and w and have the same type of singularity at $y = \mp 1$, $x=0$. Taking Fourier inversion of (2.16) and (2.17) one obtains

$$\alpha_1 s_1 (P_1 - P_2) = \frac{2}{\pi} \int_0^1 u_1(t) \sin(st)\, ds. \tag{2.18}$$

$$s^2 (P_1 + P_2) = \frac{2}{\pi} \int_0^1 u_2(t) \sin(st)\, ds. \tag{2.19}$$

Substituting (2.18) and (2.19) in (2.10) and (2.11), the following system of integral equations are obtained:

$$\frac{1}{\pi} \int_{-1}^{+1} \sum_{1}^{2} h_{ij}(t,y)\, u_j(t)\, dt = f_i(y) \qquad |y|<1, (i=1,2) \tag{2.20}$$

$$f_1(y) = \frac{\lambda^2 R}{Eh} N^{\circ}_{xy}(y), \quad f_2(y) = \frac{a^3}{D} \int_0^y V^{\circ}_x(y)\, dy. \tag{2.21}$$

where the kernels $h_{ij}(t,y)$ $(i,j=1,2)$ are given in the Appendix I. It can be shown that h_{21} is bounded for all values of t and y and the remaining kernels have a Cauchy type singularity. For example, adding and subtracting the asymptotic value of the integrand, h_{11} may be expressed as

$$h_{11}(t,y) = \lim_{|x|\to 0} \int_0^\infty \left(\frac{e^{-s_1|x|}}{s_1} + \frac{e^{-s_2|x|}}{s_2} - 2\,\frac{e^{-s|x|}}{s} \right) s \sin\{s(t-y)\}\, ds$$

$$+ \lim_{|x|\to 0} \int_0^\infty 2\, e^{-s|x|} \sin\{s(t-y)\}\, ds$$

$$= \int_0^\infty \left(\frac{s}{s_1} + \frac{s}{s_2} - 2 \right) \sin\{s(t-y)\}\, ds + \frac{2}{t-y}$$

where because of uniform convergence in the first integral limit has been put under the integral sign. After similar operation, the equations (2.20) may be written as

$$\int_{-1}^{+1} \sum_{1}^{2} a_{ij}\, u_j(t)\, dt\, (t-y)^{-1} + \int_{-1}^{+1} \sum_{1}^{2} K_{ij}(t,y)\, u_j(t)\, dt$$

$$= \pi f_i(y)$$

$$a_{11} = 2,\ a_{12} = -1+\nu,\ a_{21} = 0 \quad a_{22} = -(1-\nu)(3+\nu) \qquad (2.22)$$

where the kernels K_{ij} are given in the Appendix I.

The singular integral equations of the type (2.22) have been extensively studied (see e.g. [15]). From (2.22) and the definition of u_j it is easy to show that the fundamental function of the system is $(1-t^2)^{-1/2}$ and the index is +1. Hence the solution of (2.22) is determined within a pair of arbitrary constants. To determine these constants the condition of continuity of displacement w for $|y| > 1$, $x = 0$ is used. This condition is given by equation (2.13) and has not yet been satisfied. Referring to (2.13) and (2.14) it is seen that (2.14), which is satisfied by the choice of u_j as in (2.17), may be regarded as the second derivative of (2.13) or w in y. Thus in order to have w vanish for $|y| > 0$, u_2 must satisfy the following two conditions:

$$\int_{-1}^{+1} u_2(t)\,dt = 0, \qquad \int_{-1}^{+1} dy \int_{-1}^{y} u_2(t)\,dt = 0 \tag{2.23}$$

2.12 Solution of Integral Equations.

Noting that the fundamental function, $(1-t^2)^{-1/2}$ of the system of singular integral equations (2.20) is the weight of the Chebishev polynomials $T_n(t)$ and u_1 , u_2 are

odd functions (see 2.16, 2.17), the solution of the integral equations can be expressed in the form

$$u_1(t) = (1-t^2)^{-\frac{1}{2}} \sum_1^\infty A_n T_{2n-1}(t)$$

$$u_2(t) = (1-t^2)^{-\frac{1}{2}} \sum_1^\infty B_n T_{2n-1}(t)$$

(2.24)

where A_n and B_n are complex constants and T_n are Chebishev polynomials of the second kind.

The first condition in equation (2.23) is satisfied by the choice of u_2 as an odd function. The second condition in (2.23) gives the same result as obtained below by writing $w = 0$ at $y = \mp 1$, $x = 0$

$$0 = W(0,1) = -W(0,-1) = 2\int_0^\infty (P_1 + P_2)\, \mathrm{Sin}(s)\, ds$$

$$= 2\int_0^\infty \sin s\, ds \, \frac{2}{\pi s^2} \int_0^1 B_n (1-t^2)^{-\frac{1}{2}} T_{2n-1}(t) \sin(st)\, dt$$

$$= \frac{4}{\pi} \sum_1^\infty B_n \int_0^1 (1-t^2)^{-\frac{1}{2}} t\, T_{2n-1}(t)\, dt$$

$$= B_1$$

To determine the remaining constants A_n and B_n the technique described in [16] is used. Substituting the solution (2.24) in (2.22), the singular integrals have the form

$$\int_{-1}^{+1} \frac{T_{2n-1}(t)\,(1-t^2)^{-1/2}}{(t-y)}\,dt$$

Other integrals are of the type

$$\int_{-1}^{+1} T_{2n-1}(t)\,(1-t^2)^{-1/2}\,t^{-1}\,dt$$

$$\int_{-1}^{+1}\left\{\int_0^\infty f_2(s)\,\sin(s\overline{t-y})\,ds\right\} T_{2n-1}(t)(1-t^2)^{-\frac{1}{2}}dt$$

$$\int_{-1}^{+1}\left\{\int_0^\infty f_3(s)\,\sin(st)\,ds\right\} T_{2n-1}(t)(1-t^2)^{-\frac{1}{2}}dt$$

$$\int_{-1}^{+1}\left\{\int_0^\infty f_4(s)\,(1-\cos(sy))\,\sin(st)\,ds\right\} T_{2n-1}(t)(1-t^2)^{-\frac{1}{2}}dt.$$

Next both sides of integral equations are multiplied by $U_{2k}(y)\ (1-y^2)^{1/2}$ $(k = 0,1,2.....n-1)$ and integrated from

-1 to +1 in y, thus a system of algebraic equations are obtained for the unknown complex constants A_n and B_n. The singular integrals have the form

$$\int_{-1}^{+1}\left[\int_{-1}^{+1} T_{2n-1}(t)(1-t^2)^{-1/2}(t-y)^{-1}dt\right]u_{2k}(y)(1-y^2)^{\frac{1}{2}}dy$$

$$= \int_{-1}^{+1} \pi\, u_{2n-2}(y)\, u_{2k}(y)\,(1-y^2)^{\frac{1}{2}}dy$$

$$= \pi^2/2 \qquad \text{for } 2n-2 = 2k$$

$$= 0 \qquad \text{otherwise}$$

Other integrals have the form

$$I_1 = \int_{-1}^{+1}\left[\int_{-1}^{+1} T_{2n-1}(t)(1-t^2)^{-\frac{1}{2}}t^{-1}dt\right]u_{2k}(y)(1-y^2)^{\frac{1}{2}}dy$$

$$= \pi\int_{-1}^{+1} U_{2n-2}(y)\, u_{2k}(y)(1-y^2)^{\frac{1}{2}}dy$$

$$= \frac{\pi^2}{2}(-1)^{n-1} \qquad k=0$$

$$= 0 \qquad k\neq 0.$$

$$I_2 = \int_{-1}^{+1}\left[\int_{-1}^{+1}\left\{\int_0^\infty f_2(s)\sin(s\sqrt{t-y})\,ds\right\}T_{2n-1}(t)(1-t^2)^{-\frac{1}{2}}dt\right]\cdot$$

$$\cdot\, u_{2k}(y)(1-y^2)^{1/2}dy.$$

$$I_3 = \int_{-1}^{+1}\left[\int_{-1}^{+1}\left\{\int_0^\infty f_3(s)\sin(st)\,ds\right\}T_{2n-1}(t)(1-t^2)^{-\frac{1}{2}}dt\right]u_{2k}(y)\cdot$$

$$\cdot\,(1-y^2)^{1/2}dy.$$

$$I_4 = \int_{-1}^{+1}\left[\int_{-1}^{+1}\left\{\int_0^\infty f_4(s)(1-\cos(sy)\sin(st)\,ds\right\}T_{2n-1}(t)(1-t^2)^{-1/2}dt\right]\cdot$$

$$\cdot\, u_{2k}(y)(1-y^2)^{1/2}\,dy.$$

Integrals I_2 , I_3 and I_4 are of Gauss-Chebishev type and can be evaluated by using Reference [17]. Thus,

$$I_2 = \frac{\pi^2}{p(q+1)} \sum_{i}^{q} \sum_{1}^{p} \cos 2n\theta_i \sin\theta_j \sin(2k+1)\theta_j \int_0^\infty f_2(s) \sin s \, (\cos\theta_i - \cos\theta_j)\, ds$$

$$I_3 = \frac{\pi}{2p} \sum_{i=1}^{p} \cos 2n\theta_i \int_0^\infty f_3(s) \sin(s\cos\theta_i)\, ds \qquad \text{for } k = 0$$

$$= 0 \qquad \text{otherwise}$$

$$I_4 = \frac{\pi^2}{p(q+1)} \sum_{i=1}^{p} \sum_{j=1}^{q} \cos 2n\theta_i \sin\theta_j \sin(2k+1)\theta_j \int_0^\infty f_4(s) \left[1 - \cos(s\cos\theta_j)\right] \sin(s\cos\theta_i)\, ds$$

where $\theta_i = (2p)^{-1}(2i-1)\pi$, $\theta_j = (q+1)^{-1}\pi j$

Integrals I_2 , I_3 and I_4 are evaluated numerically by using Filon integration formula. To evaluate the infinite integrals, the integration is carried out from zero to 50 and from 50 to infinity asymptotic expansion is used to evaluate the integrals.

The right hand side of the integral equations becomes

$$\pi \int_{-1}^{+1} f_j(y)\, u_{2k}(y)\,(1-y^2)^{\frac{1}{2}}\, dy$$

This integral can be evaluated in the closed form for the values of $f_j(y)$ under consideration.

Once u_1 and u_2 are obtained, all field quantities in the shell may be expressed as infinite integrals. P_1 and P_2 are obtained by substituting (2.24) in (2.18) and (2.19)

$$\alpha_1 s_1 (P_1 - P_2) = \sum_1^\infty (-1)^{n-1} A_n J_{2n-1}(s)$$

$$s^2 (P_1 + P_2) = \sum_1^\infty (-1)^{n-1} B_n J_{2n-1}(s) \qquad (2.25)$$

The functions w and F are obtained as

$$w(x,y) = \operatorname{Sgn}(x) \int_0^\infty \sum_1^\infty (-1)^{n-1} J_{2n-1}(s) 2^{-1} \left\{ \frac{A_n}{\alpha_1 s_1} + \frac{B_n}{s^2} \right\}$$

$$e^{(\alpha_1 - s_1)|x|} + \left(-\frac{A_n}{\alpha_1 s_1} + \frac{B_n}{s^2} \right) e^{-(\alpha_1 + s_1)|x|}$$

$$+ \left(\frac{B_n}{s^2} + \frac{A_n}{\alpha_2 s_2} - \frac{(1-\nu) B_n}{\alpha_2 s_2} \right) e^{-(\alpha_2 + s_2)|x|}$$

$$+ \left(\frac{B_n}{s^2} - \frac{A_n}{\alpha_2 s_2} + \frac{(1-\nu) B_n}{\alpha_2 s_2} \right) e^{(\alpha_2 - s_2)|x|} \Bigg\}$$

$$\sin(sy)\, ds.$$

$$F(x,y) = \frac{\{Eh a^2}{\lambda^2 R} \operatorname{Sgn}(x) \int_0^\infty \sum_1^\infty (-1)^{n-1} z^{-1} J_{2n-1}(s) \Big\{ \Big(\frac{An}{\alpha_1 s_1} + \frac{Bn}{s^2} \Big) e^{(\alpha_1 - s_1)|x|} + \Big(-\frac{An}{\alpha_1 s_1} + \frac{Bn}{s^2} \Big) e^{-(\alpha_1 + s_1)|x|}$$

$$- \Big(\frac{Bn}{s^2} + \frac{An}{\alpha_2 s_2} - \frac{(1-\nu)Bn}{\alpha_2 s_2} \Big) e^{-(\alpha_2 + s_2)|x|}$$

$$- \Big(\frac{Bn}{s^2} - \frac{An}{\alpha_2 s_2} + \frac{(1-\nu)Bn}{\alpha_2 s_2} \Big) e^{(\alpha_2 - s_2)|x|} \Big\} \cdot$$

$$\cdot \sin(sy)\, ds.$$

Thus the complete solution to the problem is known. As an example, consider the torsion problem in which

$$N_{xy}^{o}(y) = N_o \quad , \quad V_x^o(y) = 0$$

Define the following auxiliary functions

$$\bar{u}_k(t) = \bar{u}_k(t)/u_o \quad , \quad u_o = \frac{N_o \lambda^2 R}{Eh} \qquad k = 1, 2$$

$$\bar{u}_1(t) = (1-t^2)^{-1/2} \sum_1^\infty a_n T_{2n-1}(t)$$

$$\bar{u}_2(t) = (1-t^2)^{-\frac{1}{2}} \sum_1^\infty b_n T_{2n-1}(t) \qquad (2.27)$$

Here $A_n = u_o a_n$, $B_n = u_o b_n$. The leading terms of the membrane and bending components of stresses around the crack tip y = 1, x = 0 are obtained as

$$\sigma_{xy}^{m} = \frac{N_{xy}}{h} = -\frac{i E u_o}{\lambda^2 R} \sum_{1}^{\infty} \left(\frac{a_n}{2} - (1-\nu)\frac{b_n}{4}\right) \frac{1}{(2\pi/a)^{1/2}}$$

$$\left(3\cos\theta/2 + \cos 5\theta/2\right) + O(1)$$

$$= \frac{N_o}{2\pi}\sqrt{\frac{a}{2\pi}}\left[-\frac{i}{4}\sum_{1}^{\infty}\left(a_n - (1-\nu)\frac{b_n}{4}\right)\right]\left(3\cos\theta/2\right.$$

$$\left. + \cos 5\theta/2\right) + O(1)$$

Defining the corresponding flat plate stress intensity factor k_p and a shell curvature correction factor C_m by

$$k_p = \frac{N_o a^{1/2}}{h} \quad , \quad \frac{k_s}{k_p} = C_m = -i \sum_{1}^{\infty} \left[2a_n - (1-\nu) b_n\right] \tag{2.28}$$

σ_{xy}^{m} and the remaining membrane stresses become

$$\sigma_{xy}^{m} = \frac{k_p C_m}{4(2\pi)^{1/2}} \left(3\cos\frac{\theta}{2} + \cos 5\theta/2\right) + O(1)$$

$$\sigma_{xx}^{m} = \frac{K_b C_m}{4(2\pi)^{1/2}} \left(5\sin 5\theta/2 - 5\sin \theta/2\right) + O(1)$$

$$\sigma_{yy}^{m} = \frac{K_b C_m}{4(2\pi)^{1/2}} \left(7\sin \theta/2 + \sin 5\theta/2\right) + O(1)$$

(2.29)

where k_s^m is the membrane component of the shell stress intensity factor and r and Θ are the polar coordinates around the crack tip y = 1, x = 0. Similarly

$$\sigma_{xy}^{b} = \frac{12 Z m_{xy}}{h^3} = -\frac{E Z u_o}{(1+\nu)a^2} \sum_{1}^{\infty} \frac{bn}{4} \left(\frac{a}{2\pi}\right)^{1/2} \left[(5+3\nu)\right.$$

$$\left.\cos \theta/2 - (1-\nu) \cos 5\theta/2\right] + O(1)$$

$$= \frac{2 Z N_o a^{1/2}}{h^2 (2\pi)^{1/2}} \left[-\frac{\sqrt{3(1-\nu^2)}}{4(1+\nu)} \sum_{1}^{\infty} bn\right]\left[(5+3\nu) \cos \theta/2\right.$$

$$\left. - (1-\nu) \cos 5\theta/2\right] + O(1)$$

or substituting z = h/2, θ = 0 and defining the bending component of the stress intensity ratio by

$$C_b = k_p^{-1} \lim_{r \to 0} (2r)^{1/2} \sigma_{xy}^b = -\left[3(1-\nu^2)\right]^{1/2} \sum_1^\infty b_n$$

$$z = h/2, \quad \theta = 0 \tag{2.30}$$

σ_{xy}^b and the remaining bending stresses may be expressed as

$$\sigma_{xy}^b = \frac{k_p C_b 2z}{(2r)^{1/2} 4h(1+\nu)} \left[(5+3\nu)\cos\theta/2 - (1-\nu)\cos 5\theta/2\right] + O(1)$$

$$\sigma_{xx}^b = -\frac{k_p C_b 2z(1-\nu)}{(2r)^{1/2} h\, 4(1+\nu)} \left[\sin\theta/2 - \sin 5\theta/2\right] + O(1)$$

$$\sigma_{yy}^b = \frac{k_p C_b 2z}{(2r)^{1/2} h\, 4(1+\nu)} \left[(9+7\nu)\sin\theta/2 - (1-\nu)\sin\frac{5\theta}{2}\right] + O(1)$$

(2.31)

(2.29) and (2.31) are, respectively, identical to the solution of a plane problem and that of a plate bending problem utilizing a fourth order theory.

For the example under consideration, i.e., a cylindrical shell containing a circumferential crack which is

subjected to uniform torsion away from the location of the crack, the membrane and bending components of the stress intensity factor ratio, C_m and C_b are given in Figure 2. These values are obtained for $\nu = 1/3$.

In practice the series in (2.24) is truncated at $n = N$, where the value of N is dictated by convergence of constants C_m and C_b . For a given accuracy in C_m and C_b , the required number N increases with increasing shell parameter λ .

In the numerical analysis presented here, integration points p and q in Gauss-Chebishev integrals are taken as 30 each. No significant difference in stress intensity factor ratios was obtained by changing p and q to 40 each. As mentioned earlier, the infinite integrals which are unbounded at zero are evaluated from small quantity ε (ε = 0.0001) to 50, and to evaluate the integrals from zero to ε and from 50 to infinity asymptotic expansions are used. No significant difference in the results was obtained by changing the lower limit of integration ε and upper limit of integration 50.

2.2 Symmetric Problem

Proceeding exactly in the same way as in the antisymmetric case (for details see Appendix I) the solution of the symmetrically loaded cylindrical shell problem containing

a circumferential crack may be reduced to that of the following system of integral equations.

$$\int_{-1}^{+1} \sum_{1}^{2} L_{ij}(t,y)\, \varphi_j(t)\, dt = f_i(y) \qquad |y|<1$$

$$i = 1,2. \tag{2.32}$$

$$f_1(y) = -\frac{n_0 \pi \lambda^2 R y}{i E h a^2}, \qquad f_2(y) = -m_0 \pi y$$

(2.33)

where $\varphi_i(t)$ are the auxiliary functions and the kernels $L_{ij}(t,y)$ $(i,j = 1,2)$ are given in Appendix II. It is assumed that the uniform normal and bending loads acting on the crack surface are the only external loads which are related to n_0 and m_0 by

$$N_x(0,y) = \frac{n_0}{a^2} \qquad M_x(0,y) = \frac{D m_0}{a^2} \qquad -1 < y < 1$$

(2.34)

All the kernels have Cauchy type singularity. For example, adding and subtracting the asymptotic value of the integrand,

L_{11} may be expressed as

$$L_{11}(t,y) = \lim_{|x|\to 0} \int_0^\infty \left[s_1^{-1} s e^{-s_1|x|} - e^{-s|x|} \right] \sin\{s(t-y)\}\, ds$$

$$- \nu \int_0^\infty \left[s s_2^{-1} e^{-s_2|x|} - e^{-s|x|} \right] \sin\{s(t-y)\}\, ds$$

$$+ (1-\nu) \int_0^\infty e^{-s|x|} \sin\{s(t-y)\}\, ds.$$

$$= \int_0^\infty \left(\frac{s}{s_1} - 1 \right) \sin\{s(t-y)\}\, ds - \nu \int_0^\infty \left(\frac{s}{s_2} - 1 \right) \sin\{s(t-y)\}\, ds$$

$$+ \frac{1-\nu}{t-y}$$

After similar operation equation (2.32) may be written as

$$\int_{-1}^{+1} \sum_1^2 a_{ij} \varphi_j(t) \frac{dt}{t-y} + \int_{-1}^{+1} \sum_1^2 R_{ij}(t,y) \varphi_j(t,y)\, dt = \pi f_i(y)$$

$$|y|<1 \qquad (2.35)$$

$$a_{11} = 1-\nu \,, \quad a_{12} = 1+\nu \,, \quad a_{21} = (1-\nu)(3+\nu), \quad a_{22} = -(1-\nu)(3+\nu)$$

where the kernels R_{ij} are given in Appendix II. From the definition of φ_j, it is easy to show that the fundamental function of the system is $(1-t^2)^{1/2}$ and the index is -1. Noting that the fundamental function $(1-t^2)^{1/2}$ of the system

of singular integral equations (2.35) is the weight of the Chebishev polynomials $U_n(t)$, and $\varphi_1(t)$, $\varphi_2(t)$ are even functions the solution of the integral equations can be expressed in the form

$$\varphi_j(t) = (1-t^2)^{1/2} \sum_0^\infty A_{jn} U_{2n}(t)$$

(2.36)

where A_{jn} (j=1,2, n=0,1,2.....) are undetermined (complex) constants and $U_{2n}(t)$ (n=0,1....) are the Chebishev polynomials of the second kind.

Substituting (2.36) in (2.35) and multiplying both sides of the equations by $T_k(y)$ $(1-y^2)^{-1/2}$ (k = 1,3,.....n) and integrating from -1 to +1 a system of algebraic equations are obtained which can be solved for the unknown coefficients A_{ij}.

Following the procedure outlined in the previous problem, the stress intensity factor ratios may be expressed as

$$B_m = \frac{k_m^s}{k_p} = -i \sum_0^\infty (n+1)\left[(1-\nu) A_{1n} + (1+\nu) A_{2n}\right]$$

$$B_b = \frac{k_b^s}{k_p} = (1-\nu) \sum_0^\infty (n+1)\left[A_{1n} - A_{2n}\right]$$

(2.37)

k_m^s and k_b^s are the membrane and bending components of the stress intensity factor in the shell. For example, ahead of the crack tip for $\theta = 0$ and at a small distance r the membrane and bending components of the stress may be expressed as

$$\sigma_\theta^m(r,0) = \frac{k_m^s}{(2r)^{1/2}} + O(1)$$

$$\sigma_\theta^b(r,0) = \mp \frac{k_b^s}{(2r)^{1/2}} + O(1)$$

where + and - signs refer to the outer and inner surfaces, respectively. In (2.37) k_p is the corresponding plate stress intensity factor.

For example, in a cylindrical shell under uniform axial tension $N_x = N_o$, $k_p = \sqrt{a\pi}/h$. The results for stress intensity factors B_m and B_b are shown in Figures 3 and 4, which also show the asymptotic solution given in [3].

The integrals in the symmetric problem are of the same type as in the anti-symmetric problem and hence exactly similar procedure is adopted to evaluate the integrals.

III. PLASTICITY AND CRACK OPENING DISPLACEMENT

In this chapter, a method for determining the plastic zone ahead of a crack tip is outlined. The model developed here is based on the concept of Dugdale's model. The particular case of cylindrical shell with a circumferential crack is considered. From the solution of the plastic zone size, the crack opening displacement is obtained for the problem under consideration.

3.1 The Plastic Zone Size

Let the actual crack length in the shell be 2a, and the plastic deformation be confined to a narrow strip of length p ahead of the crack tips (Figure 5). Define

$$a_p = a + p \quad , \quad \alpha = \frac{a}{a_p} \tag{3.1}$$

To determine the unknown constant a_p (or p) the standard procedure of removing the stress singularities at the fictitious crack tip a_p through the superposition of two solutions is followed. For simplicity, here it is assumed that outside the perturbation zone of the crack, the shell is subjected to symmetrically applied constant membrane stresses and in this region the stress resultant

which is perpendicular to the crack is N_o. The solution for a shell with crack length $2a_p$ and subjected to membrane load $N_y = -N_o$ is first obtained. This solution gives the membrane and bending components of the stress intensity factor as (see Appendix III)

$$K_I^m = A_m(\lambda_p)\frac{N_o(a_p)^{1/2}}{h}, \quad K_I^b = A_b(\lambda_p)N_o(a_p)^{1/2}h^{-1} \tag{3.2}$$

where the stress intensity factor ratios A_m and A_b are functions of λ_p only and are obtained numerically in tabular form.

Next, the shell under the external loads coming from the plastic zone lying ahead of the crack tips is considered. For this it is assumed that the crack length again is $2a_p$ and the shell is subjected to the following surface tractions at the crack surfaces:

$$\begin{aligned} &N_x = N, \quad M_x = M, && \alpha < |y| < 1 \\ &N_x = 0, \quad M_x = 0, && |y| < \alpha \\ &N_{xy} = 0, \quad V_x = 0, && |y| < 1 \end{aligned} \tag{3.3}$$

As in the most applications of the plastic strip model, here it is assumed that the unknown tractions N and M are constant. The solution of this problem gives the stress intensity factors as:

$$K_2^m = B_{11}(\alpha,\lambda_p)\frac{N}{h}a_p^{1/2} + B_{12}(\alpha,\lambda_p)\frac{M6}{h^2}a_p^{1/2}$$

$$K_2^b = B_{21}(\alpha,\lambda_p)\frac{N}{h}a_p^{1/2} + B_{22}(\alpha,\lambda_p)\frac{M6}{h^2}a_p^{1/2} \qquad (3.4)$$

where the stress intensity factor ratios $B_{ij}(i,j = 1,2)$ are calculated in tabular form as function of α and λ_p. Here B_{11} and B_{21} are membrane and bending stress intensity factor ratios when the traction is membrane load only and B_{12} and B_{22} are membrane and bending stress intensity factor ratios when the traction is bending load.

The condition that the stress intensity factor ratios should vanish at $x = \pm 1$ (i.e. at the ends of plastic zone) may now be expressed as

$$k_1^m + k_2^m = 0, \qquad k_1^b + k_2^b = 0 \qquad (3.5)$$

By using (3.2) and (3.4) and dividing by the yield strength, above relations reduce to

$$B_{11}\frac{N}{h\sigma_y} + B_{12}\frac{6M}{h^2\sigma_y} + A_m\frac{N_0}{h\sigma_y} = 0$$

$$B_{21}\frac{N}{h\sigma_y} + B_{22}\frac{6M}{h^2\sigma_y} + A_b\frac{N_0}{h\sigma_y} = 0$$

(3.6)

In the plastic strip, $\alpha < |x| < 1$, the tractions N and M are expected to satisfy some kind of yield condition. One such condition which is most commonly used may be expressed as

$$\frac{N}{h\sigma_y} + \left|\frac{6M}{h^2\sigma_y}\right| = 1$$

(3.7)

Equations (3.6) and (3.7) provide three (highly non-linear) algebraic equations to determine the unknown α, N and M. Once α is determined, (3.1) gives the plastic zone size as

$$p = a\left(\frac{1}{\alpha} - 1\right)$$

(3.8)

Eliminating N and M, (3.6) and (3.7) may be written in the following form:

$$\left[(b_{11} + b_{21}) A_m + (b_{12} + b_{22}) A_b \right] \frac{N_o}{h \sigma_y} + 1 = 0 \tag{3.9}$$

where the matrix (b_{ij}) is the inverse of (B_{ij}) (which is assumed to be non-singular). Noting that $\lambda_p = \lambda/\alpha$, (3.9) determines α as a function of the (actual) shell parameter λ and the stress ratio $N_o/h\sigma_y$. For the limiting case $\lambda = 0$, the problem is that of uniformly loaded flat plate and α is given by

$$\alpha = \cos\left(\frac{\pi N_o}{2 h \sigma_y}\right) , \quad \lambda = 0 \tag{3.10}$$

For the cylindrical shell with a circumferential crack and subjected to uniform tension away from the crack the bending component of stress intensity factor is very small as seen in Figure 4 and hence the effect of bending is neglected. The solution of the equation (3.9) is shown in Figure 6. As the stress ratio $N_o/h\sigma_y$ increases, the convergence of the numerical procedure becomes slower, and more computer time is required to calculate the α values.

This is the reason for seemingly incomplete plots in the Figure 6.

Obviously it is desired to have an analytical expression for α as a function of $N_o/h\sigma_y$ which is an acceptable approximation. For a cylindrical shell with a circumferential crack under axial tension the expression

$$\alpha = \left(\cos\frac{\pi N_o}{2h\sigma_y}\right)^{1+0.2\lambda} + 0.00854\lambda\, e^{-\lambda^3} \sin\frac{\pi N_o}{h\sigma_y} \tag{3.17}$$

seems to be quite satisfactory except for the range in which λ and $N_o/h\sigma_y$ are large ($\lambda > 3$, $N_o/h\sigma_y > 0.7$).

3.2 The Crack Opening Displacement

Referring to Figure 1, the crack opening displacement u(o,y) is given by the x-component of the displacement vector on the crack surface (at the middle surface of the shell). This is obtained from

$$\varepsilon_x = \frac{1}{Eh}\left[N_x - N_y\nu\right] = \frac{\partial u}{a_p \partial x} - \frac{w}{R_x} \tag{3.12}$$

where a_p is the half crack length used to normalize the dimensions, w is the z-component of the displacement vector, and R_x is the principal radius of curvature in x-z plane. In terms of stress function F and displacement w, (3.12) may be expressed as

$$\frac{\partial u}{\partial x} = \frac{1}{Eh a_p}\left(\frac{\partial^2 F}{\partial y^2} - \nu \frac{\partial^2 F}{\partial x^2}\right) + \frac{a_p w}{R_x} \tag{3.13}$$

For a cylindrical shell with a circumferential crack $R_x = \infty$ and the analysis is very much simplified. The function F for the symmetric problem is given in Appendix II. Substituting for F (3.13) and simplifying, the following expression for u(o,y) is obtained:

$$\frac{\chi^2 R}{2i a_p} u(o,y) = \int_o^\infty \left[(1-\nu)(P_1+P_2) S_1 + (1+\nu)(P_1-P_2)\alpha_1\right] \cos(sy)\, ds. \tag{3.14}$$

Using the definition of φ_1 and φ_2 equation (3.14) reduces to

$$\frac{\lambda^2 R}{2 i a_p}\, u(0,y) = \begin{cases} (1-\nu)\,\varphi_1(y) + (1+\nu)\,\varphi_2(y) & |y| < 1 \\ 0 & |y| > 1 \end{cases}$$

(3.15)

where u(0,y) is one-half of the crack opening displacement. The unknown functions φ_1 and φ_2 are obtained from the solution of integral equations (2.35).

When the plastic strip model is used to account for yielding around the crack tips, the crack opening displacement is defined as the relative crack opening at $y = \mp \alpha$ obtained from the superposition of the following two solutions.

1. The shell with crack length $2a_p$ subjected to the tractions

$$N_x = -N_o\,,\ M_y = 0,\ N_{xy} = 0,\ V_x = 0,\ (|y| < 1,\ x = 0)$$

(3.16)

2. Same shell subjected to tractions given by (3.3), where α, N and M satisfy the conditions (3.6) and (3.7).

Thus, the crack opening displacement δ may be expressed as

$$\delta = 2\left[u_1(0,\alpha) + u_2(0,\alpha)\right] \tag{3.17}$$

where $u_2(0,\alpha) = u_{2N} + u_{2M}$, u_{2N} and u_{2M} being the individual contributions of the loads N and M, respectively. For a cylindrical shell with a circumferential crack the bending is very small and hence u_{2M} is neglected.

Figure 7 shows some calculated results for the crack surface displacement u. The solid curve represents the displacement u(0,y) for $|y| < 1$, in a shell with parameter λ_p and subjected to uniform membrane load $N_x = -N_o$. The dashed curves u_{2N} shown in this figure are, on the other hand, obtained as the displacement at $y = \alpha$ from a solution in which $N_x = N$ applied along $\alpha < |y| < 1$, $x = 0$, is the only external load. The length parameters shown in the figures which are used to non-dimensionalize u_1 and u_{2N}, respectively, are given by

$$C_1 = \frac{N_o a_p}{hE} \quad , \quad C_N = \frac{N a_b}{hE} \tag{3.18}$$

The results given in Figure 7, with Figure 4 may be considered as a set of master curves from which the crack opening displacement δ can be calculated as a function of λ and $N_o/h\sigma_y$. It can be easily shown that

$$\frac{\delta}{d} = \frac{2}{\alpha}\left[\frac{N_o}{h\sigma_y}\frac{u_1}{c_1} + \frac{N}{h\sigma_y}\frac{u_{2N}}{c_N} + \frac{6M}{h^2\sigma_y}\frac{u_{2m}}{c_m}\right]$$

$$d = \frac{a\sigma_y}{E}$$

(3.19)

where α and the load ratios $N/h\sigma_y$ and $6M/(h^2\sigma_y)$ are obtained from the plastic strip analysis by solving (3.6) and (3.7). α is given in Figure 4.

In the limiting case of $\lambda = 0$ (i.e. the flat plate) the crack surface displacement u_1 and the crack opening displacement δ are given by

$$u_1(0,y) = 2(1-y^2)^{1/2} \qquad |y|<1$$

$$\frac{\delta}{d} = -\frac{8}{\pi}\,\mathrm{Log}\left(\cos\frac{\pi N_o}{2h\sigma_y}\right)$$

(3.20)

The numerical results for δ obtained from (3.19) and (3.20) are shown in Figure 8.

IV. FATIGUE MODELS

In this chapter the fatigue models used to fit the experimental data are reviewed.

The variety of fatigue crack propagation models which have been appearing in the literature for some time with certain regularity may be classified into four different categories, namely, (a) the models based on the microstructural theories, including the fourth power dislocation models, (b) models based on the thermal fluctuations, (c) mechanical models based on the continuum considerations, and (d) the empirical models. If one carefully examines the great majority of proposed models and the results of fatigue experiments, certain common features and trends may easily be detected. It appears that, without any reference to its rationality, the stress intensity factor is the most widely used correlation parameter in analyzing the fatigue crack propagation results. In doing so, all of the available experimental data ranging from 10^{-7} to 10^{-3} in/cycle seem to fall on an "S-shaped" curve or band in log (ΔK) vs. log (da/dn) plot, where ΔK is the amplitude of the stress intensity factor and da/dn is the crack propagation rate. Again, the examination of the results of more carefully conducted experiments indicates that as the ratio

$K_{mean}/\Delta K$ is increased, this S-shaped band seems to shift towards the higher da/dn values.

In some fatigue studies the objective is simply to exhibit the data in a coherent fashion. For this purpose all one needs is a proper correlation parameter which brings a certain degree of order to the data. However, if one intends to make any quantitative comparison or to use the results as a means of prediction (say, in designing structural components) one needs a convenient analytical model. In the case of fatigue crack propagation it is preferable that such a model should fulfill certain requirements, the important ones being (a) the model must be sufficiently simple, contain only those field quantities which are readily available or can be obtained by means of relatively simple laboratory experiments, and (b) it must conform to the basic established trends of the experimental data.

As stated earlier, as a correlation parameter the stress intensity factor amplitude is quite satisfactory. It is being used very widely and is also used in this study. One of the objectives of the present study is to demonstrate the fact that the fatigue crack propagation behavior of the shells can be predicted from that of flat plates. Hence, an analytical model is needed to be used as a basis of comparison. The fatigue models which are presented and used

in this study are basically empirical, even though one may try to rationalize and claim that they are based on certain physical principles (see, for example [18]).

The first model presented here is the generalized version of the model given in [19], and may be expressed as

$$\frac{da}{dn} = \frac{C(1+\beta)^m (\Delta\bar{K})^\alpha}{K_c - (1+\beta)\Delta\bar{K}} \tag{4.1}$$

where a is the half crack length, n is the number of cycles, C, m, α are material constants to be determined experimentally, K_c is a critical stress intensity factor, and $\Delta\bar{K}$ and β are defined by

$$\Delta\bar{K} = (\bar{K}_{max} + \bar{K}_{min})/2$$

$$\beta = (\bar{K}_{MAX} + \bar{K}_{MIN})/(\bar{K}_{MAX} - \bar{K}_{MIN}) \tag{4.2}$$

In (4.1) and (4.2) $\bar{K}$ stands for an equivalent stress intensity factor which is necessary to introduce in case of combined load conditions. For example, if the material is

subjected to combined membrane and bending loads in the vicinity of the crack tip (which is always the case in shells), and if the corresponding stress intensity factors are K_m and K_b, then $\overline{K}$ may be expressed as [18]

$$\overline{K} = K_m + K_b/2 \tag{4.3}$$

In the cylindrical shell containing a circumferential crack of length 2a and subjected to uniform longitudinal stress outside the perturbation zone of the crack

$$K = (B_m + B_b / 2)\ \sigma_x^{\infty}\ (\pi a)^{1/2} \tag{4.4}$$

where the stress intensity factor ratios, B_m, B_b are obtained from the solution of the shell equations in Chapter II and are given in Figures 3 and 4. The amplitude and the mean of $\overline{K}$ are in turn determined by using that of σ_x^{∞} in (4.4).

In (4.4) the denominator is $K_c - \overline{K}_{max}$. Hence, K_c here is a "critical stress intensity factor" at which the crack propagation rate becomes theoretically infinite (or very large). This very satisfactorily accounts for the

bend in the experimental data observed at the higher ΔK values (see Figure 10). It is obvious that K_c is related in some way to plane stress fracture strength of the material. If one may be bold enough to define such a thing as a critical stress intensity factor for plane stress fracture, the first thing one notices is that, under fixed environmental conditions, the elastic stress intensity factor (K_q) on the onset of rapid fracture is very heavily dependent on the crack length, plate thickness and plate width (see, for example, Figure 11 for the cylindrical shell with a circumferential crack). Furthermore, none of the existing plasticity correction models (e.g. [20], [21] and [22]) seem to be satisfactory to normalize the results if the net section stress to yield strength ratio is above 0.8 (which is the case in all the experiments on shells performed in this study). In the analysis of the fatigue crack propagation data reported here the constant K_c is selected in such a way that the standard error in representing the entire data in the form of (4.1) is minimum. For 6061-T4 shells this value (i.e. K_c = 44,500 psi $\sqrt{in}$) roughly corresponds to the elastic stress intensity factor at the onset of rapid fracture

for the largest crack tested (Figure 11).*

Now a second model is presented in an attempt to account for the behavior of the experimental crack growth data at the very low $\Delta \bar{K}$ values. The model is based on the notion that there is indeed a threshold value of $\Delta \bar{K}$ at which the fatigue crack propagation rate is practically zero. If this value is defined by K_T, (4.1) may be modified as**

$$\frac{da}{dn} = \frac{C_1 (1+\beta)^{m_1} (\Delta \bar{K} - K_T)^{\alpha_1}}{K_c - (1+\beta)\Delta \bar{K}} \qquad (4.5)$$

---

*Obviously one should not read too much into this statement. However, one thing seems to be clear which is that the K_c value to be used in (4.1) is much lower than the plane stress fracture toughness defined in terms of the plasticity correction models, and is rather of the order of elastic K value computed at the onset of rapid fracture. Considering the fact that the amplitude and the mean stress intensity factor used in the fatigue model are computed from the elastic theory, this may also make more physical sense.

**In both models (4.1) and (4.5) the denominator was also raised to constant power, p, which was obtained from a least square fit along with C, m and α. However, it was found that the standard error was insensitive to p (as well as to m), and p = 1 gave an error which was very close to the minimum. Thus, for the sake of simplicity, p is excluded from the models.

The theoretical curves obtained from (4.5) by using the empirical constants C_1 , m_1 and α_1 of the 6061-T4 aluminum (with K_C = 44,500 psi $\sqrt{in}$ and K_T = 500 psi $\sqrt{in}$) are shown in Figure 12 for various values of β . From Figures 10 and 12 it is evident that the theoretical curves obtained from (4.1) and (4.5) are respectively asymptotic to a straight line with a constant slope α as $\Delta\overline{K} \to 0$, and to the line $\Delta\overline{K} = K_T$ as $\Delta\overline{K} \to K_T$.

V. TEST PROCEDURE

5.1 Objectives

The purpose of the testing program was two-fold. First, to obtain fatigue crack growth and fracture data from circumferentially cracked cylindrical shells subjected to axial tension and the corresponding data from flat plates of the same material and thickness loaded uniaxially in tension. Second, to compare the crack propagation rates in plates and shells under controlled and uncontrolled environment.

5.2 Equipment

Dynamic loading on the specimen was supplied by a MTS hydraulic control system consisting of control panel, hydraulic power supply, pressure control manifold, and a 10 kip load frame. A function generator in the control panel provided the shape and rate of the loading curve. The mean stress and stress amplitude were provided by the control panel's set point and span controls.

The 10 kip load frame was calibrated to an accuracy of better than 1% of the command load on the control panel. A 50-power Gaertner travelling microscope with a 4-inch

travel was used for crack length measurements. The micrometer scale had a smallest division of 5×10^{-5} inches.

A Budd strain indicator with an accuracy of 0.1% of the reading was used for static strain measurements.

For tests under one hundred per cent humidity, distilled water was used and for tests under zero per cent humidity indicating type drierite was used to absorb moisture.

Gripping device used for shells is shown in Figure 9.

5.3 Test Materials

For comparing fatigue data in plates and shells 6061-T4 plates and shells were used. The properties of the materials and the number of specimen tested under various atmospheric conditions are given in Table I.

5.4 Flat Plate Tests

Artificial cracks were initiated, at right angles to the rolling direction in the center of each specimen by drilling a 0.04 inch diameter hole. Using a jeweler's saw, the sides of the hole were extended and then the ends of the saw cuts were tapped lightly with a razor blade to further sharpen the crack. Thus the overall length of the

crack was approximately 0.2 inch. After fabricating the artificial crack, the surface around the crack was polished with polishing compound to remove rough edges and to make the crack tips more distinguishable. Fatigue data was recorded after natural fatigue cracks had extended the overall length of the crack to 0.25 inch so that the stresses in the neighbourhood of the crack tips were not affected by the hole and saw cut.

Each plate was cycled at 10 cycles per second with sinusoidal load. The mean and range loads were fixed by the set point and span of controls of the MTS machine. Crack length versus number of load cycles data was recorded throughout each test by stopping the fluctuating load at the end of certain load cycles and measuring the crack length with a microscope while the mean load was being maintained on the plate. It was found that as crack lengths approached 1.8 inches, the sheets began to buckle in the center and hence all the fatigue tests stopped at crack length of 1.6 inches in case of tests under environments prevailing in the laboratory. For tests under one hundred per cent humidity and approximately zero per cent humidity the tests were stopped at crack length of 0.8 inch as the corresponding tests on shells were also conducted up to crack length of 0.8 inch.

Tensile test specimen were cut from the 6061-T4 sheet to obtain the material properties of the sheet.

For tests in distilled water and approximately zero per cent humidity, one side of the crack was sealed by placing two layers of thin plastic patch, one 2 inches by 2 inches and the other 3 inches by 3 inches. A 1-inch by 1-inch portion of the inner patch was kept free of the glue so that it did not stick to the plate and hence did not affect the crack growth. A plexiglass bottle 2 inches in diameter and 3 1/2 inches in height was cut in two halves and one half was glued on the other side of the crack, thus, making it possible to see the crack during fatigue cycling. For tests in distilled water the glued half of the bottle was filled with distilled water. No leakage was observed during fatigue cycling. For tests under approximately zero per cent humidity the glued half of the bottle was half filled with drierite and the top of the bottle was sealed. The specimen was kept for two days and then testing was started, thus approximately zero per cent humidity was obtained. No change in the color of drierite was observed, thus indicating that there was no leakage of moisture in the system.

5.5 Cylindrical Shell Tests

The 6061-T4 cylinders were purchased in 12-feet lengths and cut to 14 inches length to get the required size. The thickness of the cylinders was found to vary by 0.001 inch while the outside diameter varied by approximately 0.01 inch.

Tensile test specimen were cut from several cylinders to determine properties.

A fatigue crack was initiated in the center of each specimen in the same way as described for plates. The overall length of each artificial crack was approximately 0.16 inch. Fatigue data was recorded after natural fatigue cracks had extended the overall length of the crack to about 0.22 inch. The cylinders were mounted in grips shown in the Figure 9.

For one specimen four strain gauges were placed symmetrically around the circumference of the cylinder at 2 inches from the grips and four strain gauges were placed around the circumference at the place where artificial crack was initiated. These strain gauges being placed away from the crack. Strain readings were recorded under static load for various crack lengths. The crack lengths being increased by sawing the crack. It was found from the strain gauge readings that up to 0.8 inch crack length there was no detectable bending in the shell. Hence, for

fatigue tests, all data was recorded up to the crack length of about 0.8 inch.

In fatigue tests, β varied from 0.67 to 2. Thus the minimum stress went up to 2000 psi compression for $\beta = 0.67$. No buckling was observed in the cylinders. In fact, for one specimen tested, the buckling load for the shell with 0.8 inch crack was found to be 8000 psi and the buckling took place near the grips.

Fatigue data was recorded exactly in the same manner as for plates. For tests under approximately zero per cent humidity and one hundred per cent humidity exactly the same arrangement as described for plates was adopted.

After the fatigue experiments the cylinders were ruptured by slowly increasing the axial load. At one end of the crack, slow crack growth was measured by putting ink near the crack tip and measuring the distance by which the ink had advanced in the crack surface after the rupture. At the other end of the crack, the cross-hair of the microscope was moved as the crack tip moved under the application of the load. Thus slow crack growth was measured. There was no significant difference in slow crack growth obtained by two methods. The average of two readings obtained from the ink test and observation with microscope were taken as slow crack growth.

VI. DISCUSSION OF THE RESULTS

The theoretical solution of the symmetric and anti-symmetric problems provided extension and bending stress intensity factors for axial tension and torsion cases. In Chapter III, a model for plastic zone size ahead of a crack was developed and using this model crack opening displacement was obtained. The experimental program described in Chapter V provided considerable amount of fatigue crack propagation and fracture data for uniaxially stressed shells and plates. Several of salient features of the theoretical and experimental work will be discussed in the following sections.

6.1 General Considerations of the Theoretical Shell Solution

The method of obtaining Cauchy singularities in integral equations as described in Chapter II is a general one. It can be applied to any type of problem. This can be used very effectively for orthotropic shells, where the solution to the characteristic equation of the differential equations cannot be found in closed form.

By evaluating the integrals by Filon integration formula from zero to 50 and using the asymptotic expansions from 50 to infinity, it was possible to obtain a

solution to the problem up to the values of shell parameter $\lambda = 10$. Solution could be obtained even for higher values of λ by this method. However, more computer time will be required because of slow convergence. This has a distinct advantage over the method described in [24], where, Kelvin functions were used to evaluate the integrals and the solution was obtained up to $\lambda = 8$ for a cylindrical shell with an axial crack and up to $\lambda = 5.5$ for a spherical shell with a meridional crack.

For the symmetric problem of a cylindrical shell with a circumferential crack the magnitude of stress intensity factors in extension and bending is less than that found for the cylindrical shell with an axial crack. For the symmetric and anti-symmetric problems considered here, the membrane component is practically identical in the two cases. This can better be seen from Table II in which the stress intensity factor ratios for the shell under axial tension and that under torsion are tabulated. However, the table also shows that the bending stress intensity factor ratios B_b and C_b corresponding to the symmetric and anti-symmetric cases are considerably different, even though they are both small compared to the membrane components.

Figure 6 shows the relation between α and $N_o/h\sigma_y$ for various values of α. It is evident from the figure

that for shells the size of plastic zone is much larger than that for flat plates (α = 0) for the same value of N_o/h σ_o . The same trend is evident for crack opening displacement from Figure 8.

6.2 Fatigue Results Under Uncontrolled Environments

For the purpose of comparing shell and plate results under the environments prevailing in the laboratory at the time of experiments, only the part of data for which $\beta \geq 1$ is considered. For K_c = 44,500 psi$\sqrt{in}$, the material parameters obtained by using (4.1) are shown in Table III. In applying (4.1) for the curve fit the error is minimized with respect to C and α for the fixed value of m. It is felt that, to be practical, the model should not have more than two undetermined constants. The table indicates that the exponent for plates is slightly higher than that for shells. As a result, since the experimental plate and shell data practically coincide, C values for plates are considerably lower. The standard error (SE) shown in the table correspond to α = 3.5. The differences between these and the standard errors obtained for calculated exponents are very small. Hence for practical applications α as well as m may be fixed. For the crack growth rates under consideration and at room temperature and humidity α = 3.5 seems to be a very satisfactory

number for aluminum alloys. As seen from Table III, once α is fixed, variation in m does not seem to have a significant effect on the results. As an example, Figure 10 shows the experimental and theoretical results for a given value of load ratio, $\beta = 2$. The theoretical curve is obtained from (4.1) by using $m = 2$, $\alpha = 3.5$ and $C = 1.921 \times 10^{-15}$ psi $\sqrt{\text{in}}$. The figure also shows the critical value of K obtained from $(\Delta K)_c = K_c/(1+\beta)$.

The results seen in Table III are obtained from 11 shell specimens with $1 \leq \beta \leq 2$, and 25 plate specimen with $1.05 \leq \beta \leq 3.5$. It is seen that for fixed exponents m and α , the constants C obtained for shells and plates are in good agreement. Hence the fatigue crack propagation results obtained from the flat plates may be used with a certain degree of confidence to predict the fatigue behavior of shells. For $2/3 \leq \beta \leq 2$ the shell data are also analyzed by using the new model given by (4.5). In this case too, the effect of the exponent m_1 is found to be insignificant. Thus in the theoretical curve shown in Figures 12 to 14, m_1 is taken to be unity. Since the data discussed here does not cover very low crack growth range (i.e., 10^{-8} to 10^{-7} in/cycle, or lower), the standard error in the curve fit is not significantly affected by the values of K_T. The program was run for K_T values varying between

300 and 1500 psi $\sqrt{in}$. The best results were obtained for K_T = 500 psi $\sqrt{in}$. If one follows the suggestion made in [23] that the threshold value of ΔK may have something to do with endurance limit of the material, using the natural flaw size of the material in the penny-shaped crack formula one could obtain an estimate of K_T (i.e., $K_T = 2\sigma_e\sqrt{a_o/\pi}$, where σ_e is the endurance limit in fully reversed extension test and $2a_o$ is the flaw size). According to this reasoning, K_T value used here roughly corresponds to σ_e = 10,000 psi and a_o = 0.002 in. However, very careful studies are needed before this notion is taken seriously.

For $2/3 \leq \beta \leq 2$, K_c = 44,500 psi $\sqrt{in}$, K_T = 500 psi $\sqrt{in}$, $m_1 = 1$, the least square curve fit gives the remaining constants in (4.5) for 6061-T4 cylinders as

$$\alpha_1 = 2.96, \quad C_1 = 6.55 \quad 10^{-13}$$

Using these values and the proper value of β, Figures 13, 14, and 15 show the theoretical curves obtained from (4.5) superimposed on the experimental data. The figures also show the asymptotes K_T and $(\Delta K)_c$. Figure 12 shows the

crack growth data obtained from 13 specimens and a theoretical curve obtained from (4.5) with $\beta = 1.38$, which is the weighted average of values varying from 2/3 to 2. As to how well the model represents the actual data for a fixed value of load ratio may be seen from Figures 14 and 15 which show the experimental data and the theoretical curves for the two extreme values of β, namely 2 and 2/3.

6.3 Fracture tests

In fracture tests, even though the net section stress in all cylinders was above the 0.2% offset yield strength, after an initial slow growth, the unstable rapid crack propagation was clearly observed in all cases. Denoting by a_c the half crack length at the onset of rapid crack propagation and by a_o the initial length, the relationship between slow crack extension and a_o is shown in Figure 16. It is seen that the ratio $(a_c - a_o)/a_o$ over the range of crack lengths tested is approximately constant. The elastic stress intensity factor computed from

$$K_{q_f} = (B_m + B_b)\, \sigma_x^{\infty} \sqrt{\pi a_c}$$

by using the rupture stress turned out to be highly dependent on a_c, and is shown in Figure 11.

An attempt was made to give a certain degree of order to the rupture results and come up with a quantity which may be considered as a material parameter for plane stress condition by using the techniques described in [20], [21], [22] and some variations of them. However, no useful results were obtained. The model developed for plastic zone size and crack opening displacement in Chapter III could not be applied here as σ_x^{∞} at rupture in all cylinders was above the yield strength (in some cases, as much as 12%).

6.4 Fatigue Results Under Controlled Environments

For the purpose of comparing shell and plate fatigue data under controlled environments, the tests were conducted at mean stress of 12,000 psi and $\beta = 2.0$. For $K_c = 44{,}500$ psi $\sqrt{\text{in}}$, the material parameters obtained by using (4.1) are shown in Table IV. The table also shows the material parameters under controlled environments for $\beta = 2.0$ and $\bar{\sigma}_{mean} = 12{,}000$ psi.

It is seen that experimental plate and shell data practically coincide under various environmental conditions. Thus, indicating that the fatigue crack propagation in shells can be predicted from that of plates under various environmental conditions if the stress intensity

factor ratios for cracked shells are known.

It is also seen that the material constant C (normalized to α = 3.5) in uncontrolled environments and distilled water are practically the same. However, there is considerable difference in constants obtained in distilled water and approximately zero per cent humidity.

The fatigue data in normal environment prevailing in the laboratory, distilled water and approximately zero per cent humidity (for β = 2.0) for both plates and shells are shown in Figures 17 and 18.

VII. CONCLUSIONS AND SUGGESTIONS FOR FUTURE RESEARCH

7.1 Conclusions

In Chapter II the solution for symmetric and anti-symmetric problems of cylindrical shells with a circumferential crack were presented. The solutions are valid for linear elastic materials and for shell geometries which allow the application of shallow shell theories.

In Chapter III a model for the plastic zone size ahead of a crack tip was obtained. Using this model crack opening displacement was obtained. This model is applicable to cases where $N_o/h\,\sigma_y$ and λ are small ($\lambda \leq 3.0$, $N_o/h\,\sigma_y < 0.7$).

The objective of the experimental program was to determine if the fatigue and fracture properties of cylindrical shells containing a circumferential crack can be predicted from the corresponding flat plate data. It was further desired to determine if the humidity had any significant effect on fatigue crack propagation.

The results of the theoretical investigations of Chapter II indicate that

(1) The shell analysis provides stress intensity factors for the symmetric and anti-symmetric cases which are applicable for a large range of shell parameters (up to $\lambda = 10$).

(2) The analysis given is based on an eighth order shell theory in which Kirchhof assumption is made regarding the transverse shear and the twisting moment on the boundaries, including the crack surface. If a tenth order theory is used to account for all the boundary conditions separately, one would expect a shell thickness effect on the bending component, as well as a slight change in the membrane component of the stress intensity factor. The former effect is observed in [25] for the bending of flat plates where it is found that for practical values of thickness to crack length ratio h/2a, the bending stress intensity ratio varies between 0.62 (h/2a = 0) and 0.85 (h/2a = 1.5).

(3) The method of solving crack problems in shells described here is a general one and is also applicable to orthotropic shells.

(4) The analysis provided here for plastic zone size and crack opening displacement is useful for $N_o / h\sigma_0 \leq 0.7$ and $\lambda \leq 3.0$.

(5) In cylindrical shells with a circumferential crack, the size of the plastic zone ahead of the crack tip and the crack opening displacement are considerably larger than those in flat plates.

(6) For analyzing and comparing the fatigue crack propagation results in plates and shells, models given by (4.1) or (4.5) using the elastic stress intensity factors seem to be quite satisfactory. In a wide range of crack growth rates, these models may also be used quite effectively as prediction tools in design. For this purpose it is sufficient to run a series of simple plate experiments to determine the necessary material parameters which appear in the model.

(7) For 6061-T4 aluminum, within crack growth rates of 10^{-6} to 10^{-5} in/cycle, there is not much difference in fatigue crack propagation rates in distilled water and those in the uncontrolled environments prevailing in the laboratory. However, there is considerable difference in fatigue crack propagation rates under uncontrolled environments and dry environments. The difference in crack propagation rates in distilled water and dry environment is of the order of 2. Similar effects have been observed by Hartman [26] in 2024-T3 alclad sheets, by Bradshaw and Wheeler [27] in alclad aluminum-copper magnesium type alloy (DTD 5070A) and by R. P. Wei [28] in 7075-T651 aluminum.

The present observation of environment-enhanced fatigue crack growth is for plane stress. Specimen thickness will have considerable effect on crack growth rate. This effect has been investigated by R. P. Wei [29] where the possible mechanism of environment enhanced fatigue is also discussed.

(8) In the presence of significant plastic deformation around the crack tips, the fracture of the "thin-walled" structure may be analyzed by using either the plasticity-corrected stress intensity factor, K_p , or the crack opening displacement, δ . For cylindrical shells with a circumferential crack it was not possible to analyze the experimental data presented here as the stress at rupture of shells was close to yield strength or even more than yield strength in certain cases. None of the plasticity corrections mentioned in the literature seem to work.

In [20] the model for plastic zone size and crack opening displacement is developed for cylindrical shells with an axial crack. For fracture data of cylindrical shells with an axial crack given in [31] it is shown in [30] that there is an apparent improvement in the correlation of the data if the plasticity correction is used.

For the same data crack opening displacement is also obtained. Comparing the trend of the data, δ = constant appears to be a more acceptable fracture criterion. Thus, on the basis of this limited experimental verification, one may tentatively conclude that, until a better criterion for a plane stress fracture is developed, δ = constant may serve as a satisfactory model.

7.2 Suggestions for Future Research

The following are several suggestions for future research which is the logical extension of this study.

(1) Obtain the anti-symmetric solutions for a cylindrical shell with an axial crack and a spherical shell with a meridional crack.

(2) Obtain model for plastic zone size ahead of a crack tip in a cylindrical shell with a circumferential crack under torsion.

(3) Extend the present method of shell analysis to orthotropic shells.

(4) Verify the model for plastic zone size ahead of a crack tip and crack opening displacement for a cylindrical shell with a circumferential crack experimentally.

(5) Study the fatigue crack propagation in spherical shells with meridional crack experimentally.

(6) Verify the fatigue models for shells of different radii, wall thicknesses and materials.

(7) Study the fatigue crack propagation in orthotropic shells.

(8) Study the effect of mean stress on threshold value of K (i.e. K_T).

(9) Develop a model for crack opening displacement in spherical shells.

(10) Solve the problems of shells with cracks using the tenth order shell theory.

FIGURES AND TABLES

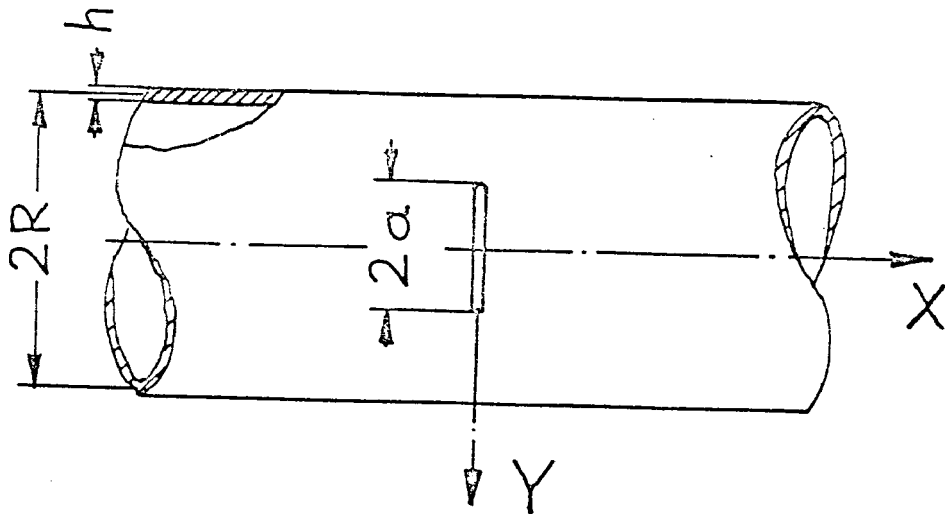

Figure 1. The geometry and loading

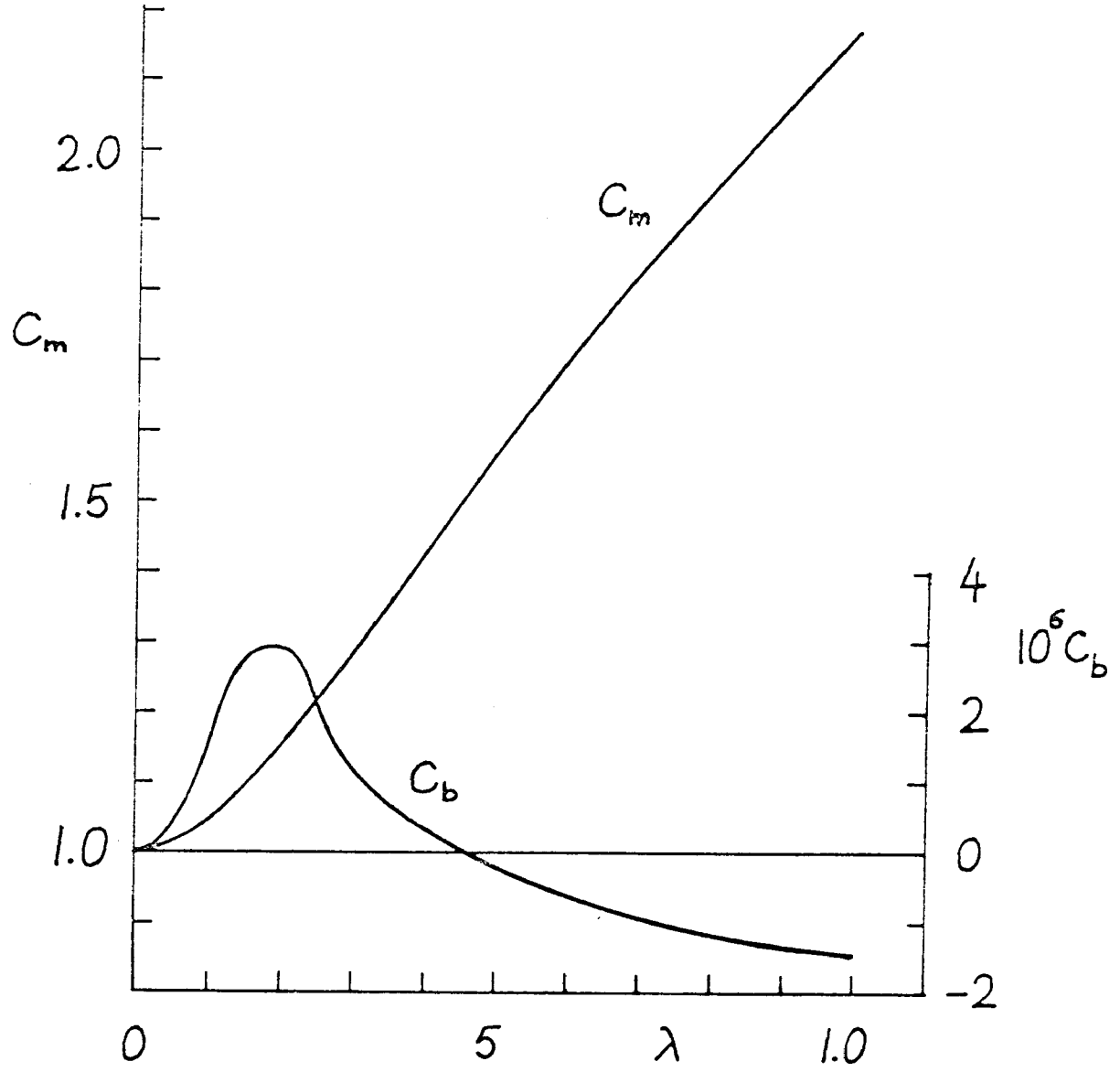

Figure 2. The stress intensity factor ratios

$$C_m = k_s^m/k_p \ , \ C_b = k_b^m/k_p$$

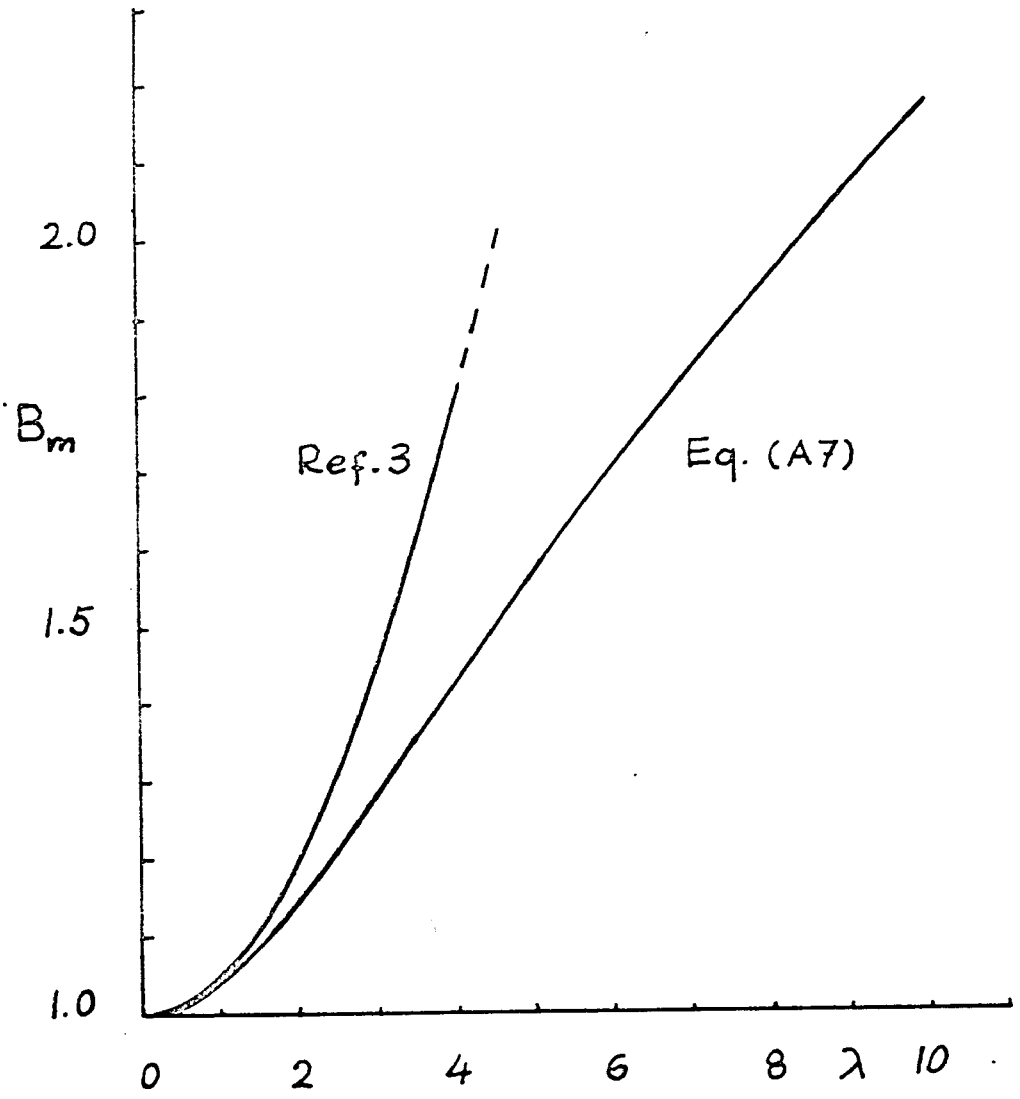

Figure 3. Membrane component of the stress intensity factor ratio

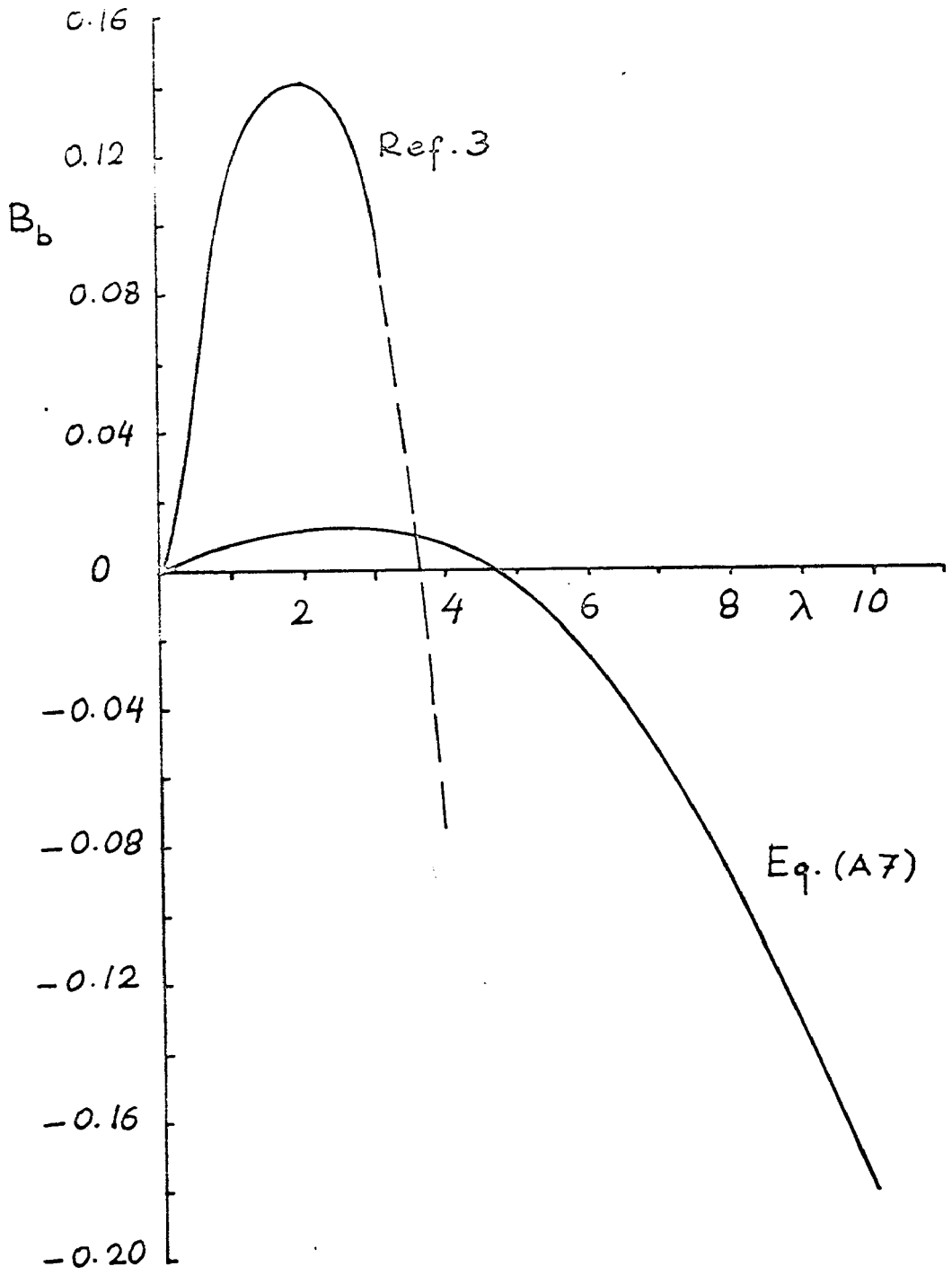

Figure 4. Bending component of the stress intensity factor ratio

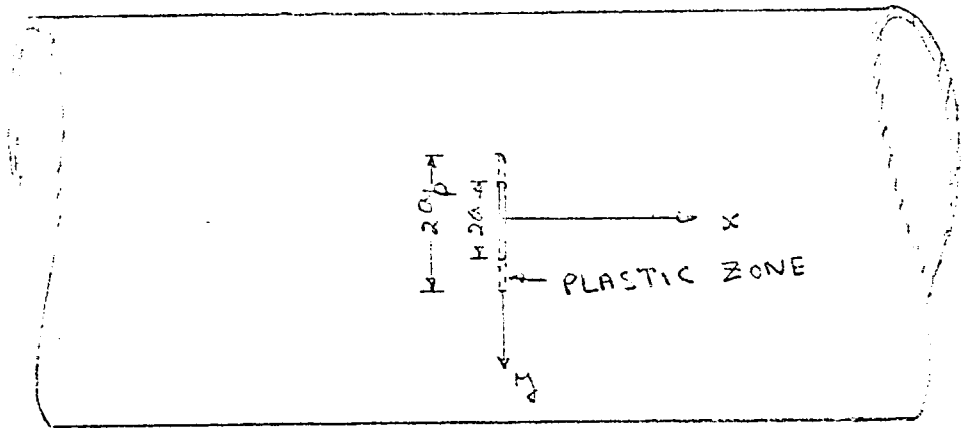

Figure 5. Crack geometry with loads acting in the plastic zone

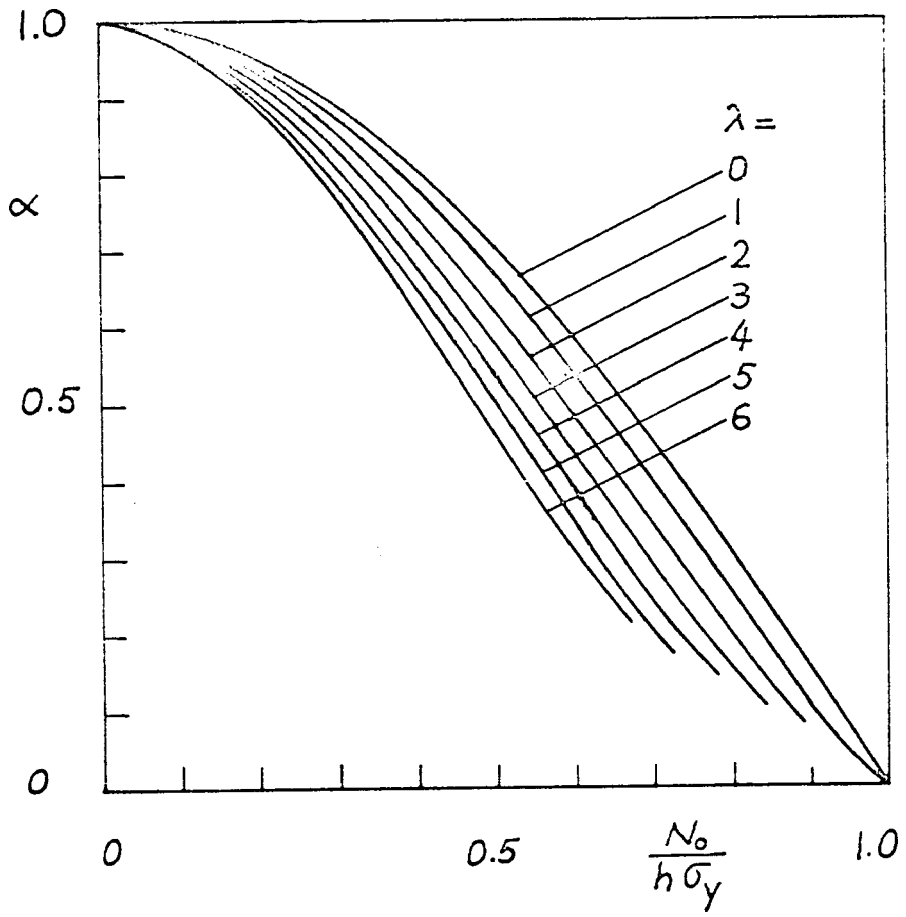

Figure 6. α vs. $N_o/(h\sigma_y)$ in cylindrical shells with a circumferential crack

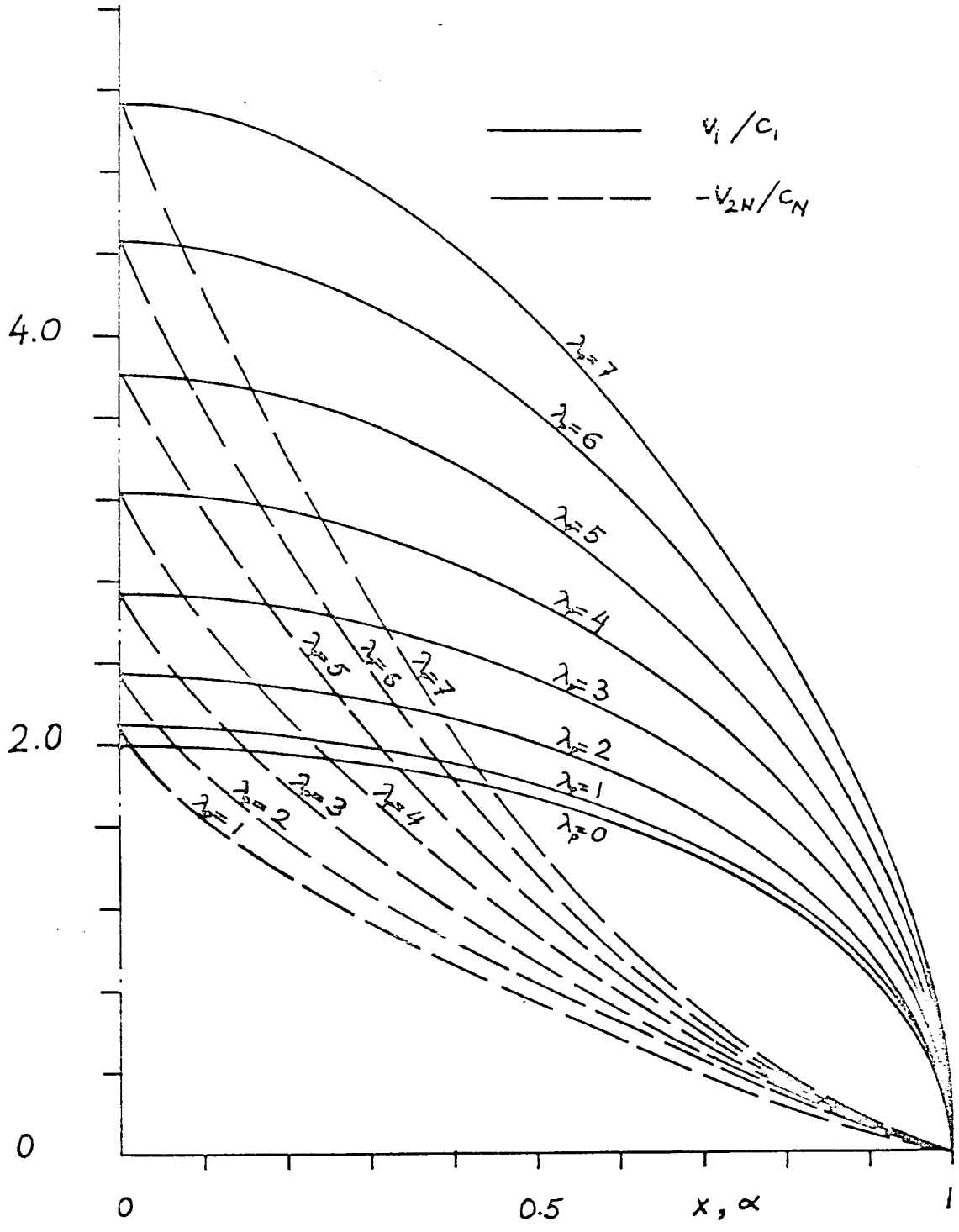

Figure 7. Crack surface displacements in cylindrical shells with a circumferential crack under membrane loads

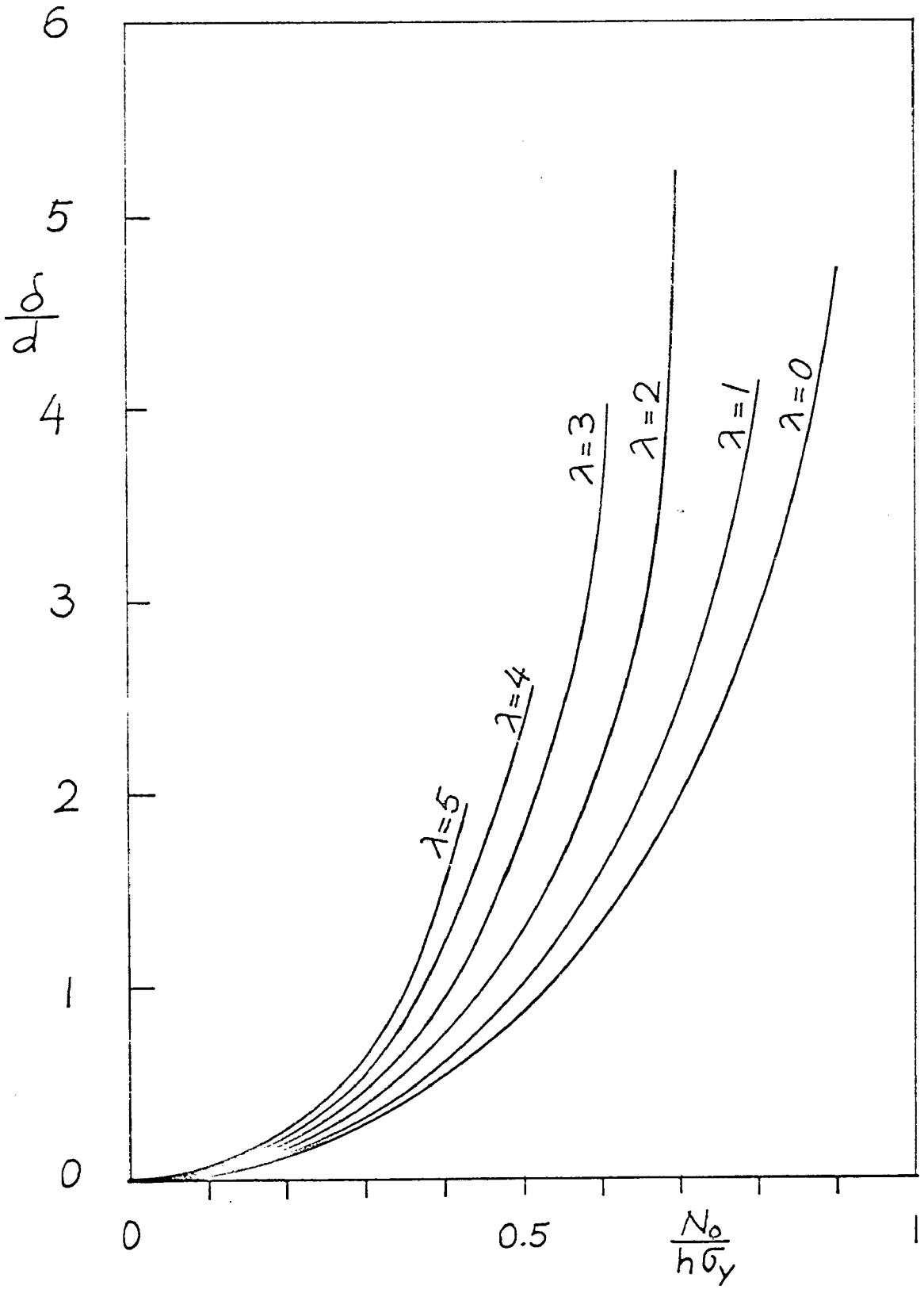

Figure 8. Crack opening displacement in cylindrical shells with a circumferential crack

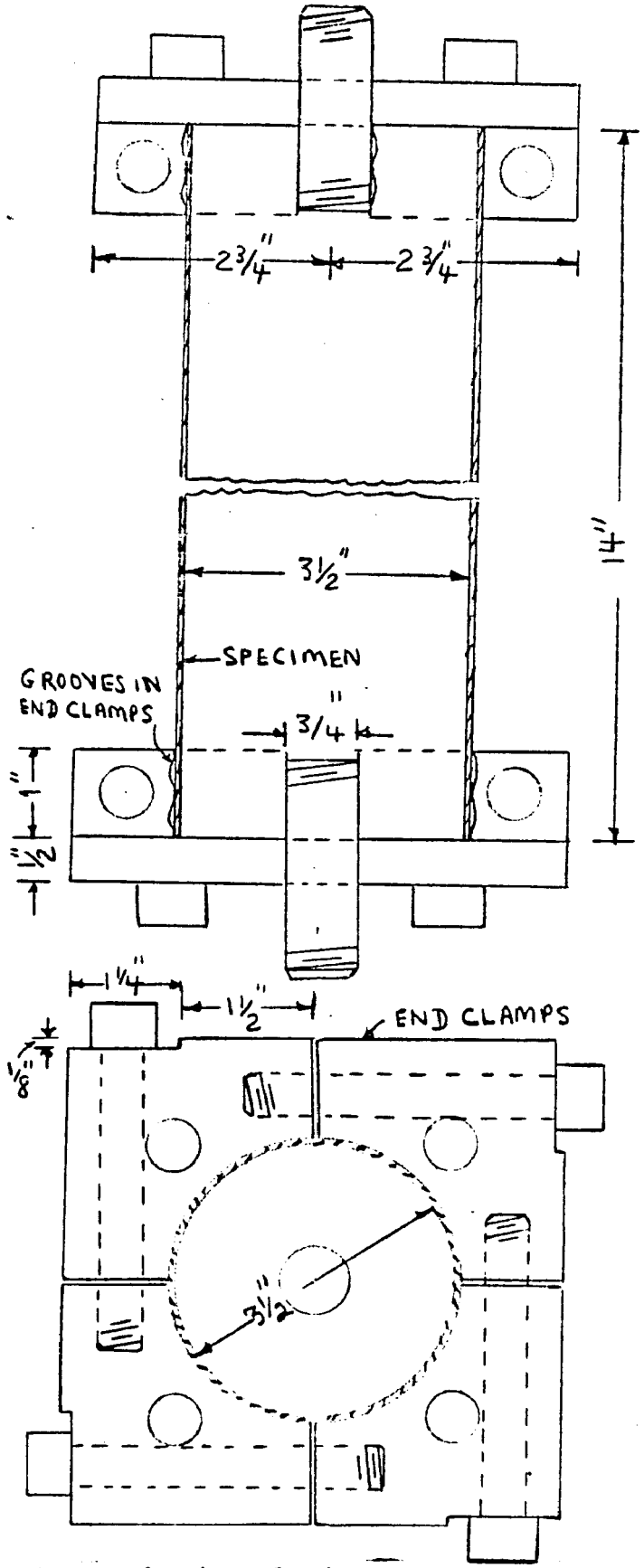

Figure 9. Gripping device for cylindrical shell specimen

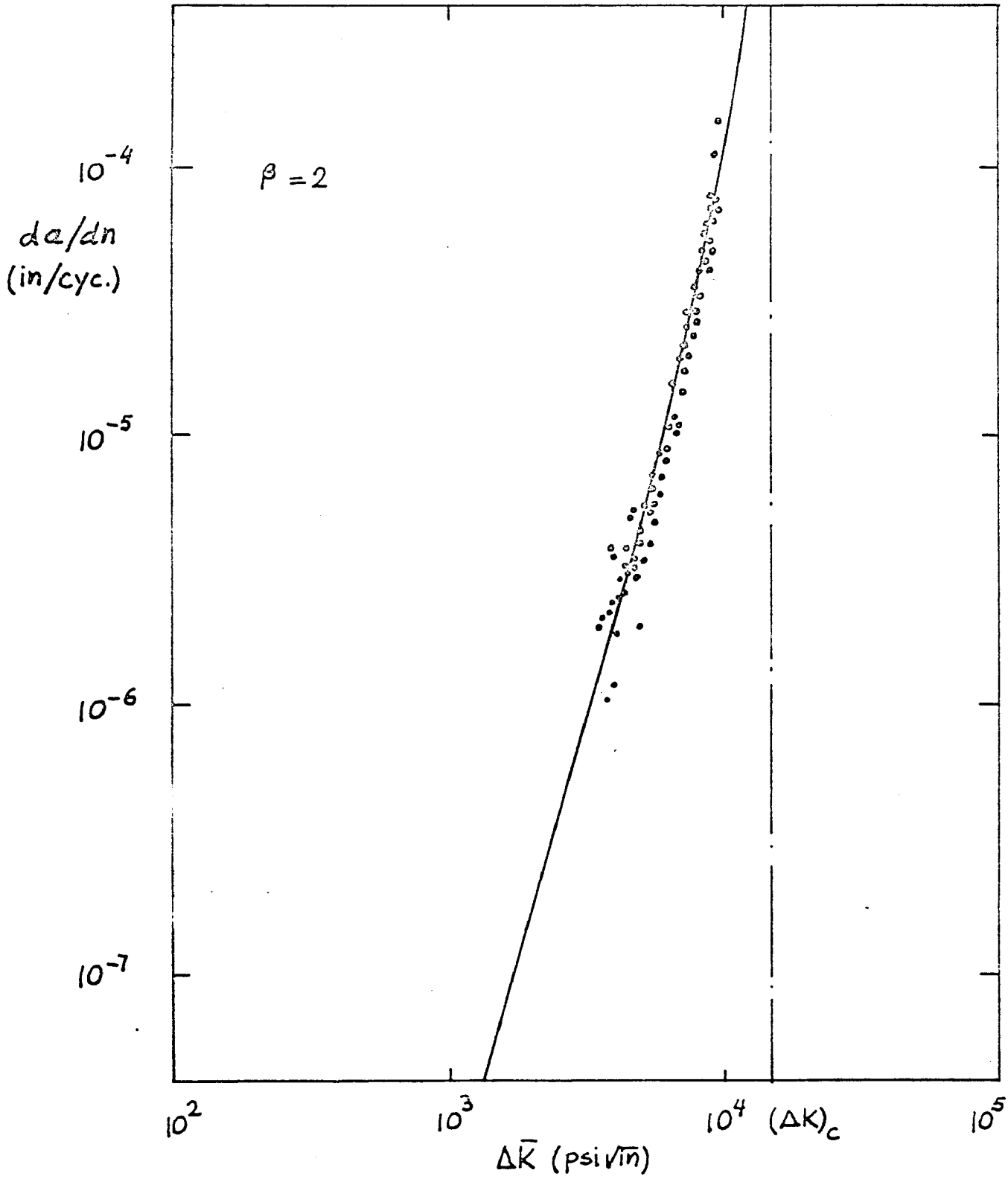

Figure 10. Fatigue crack propagation rate in 6061-T4 cylindrical shells for $\beta = 2$. The solid line is obtained from equation (1).

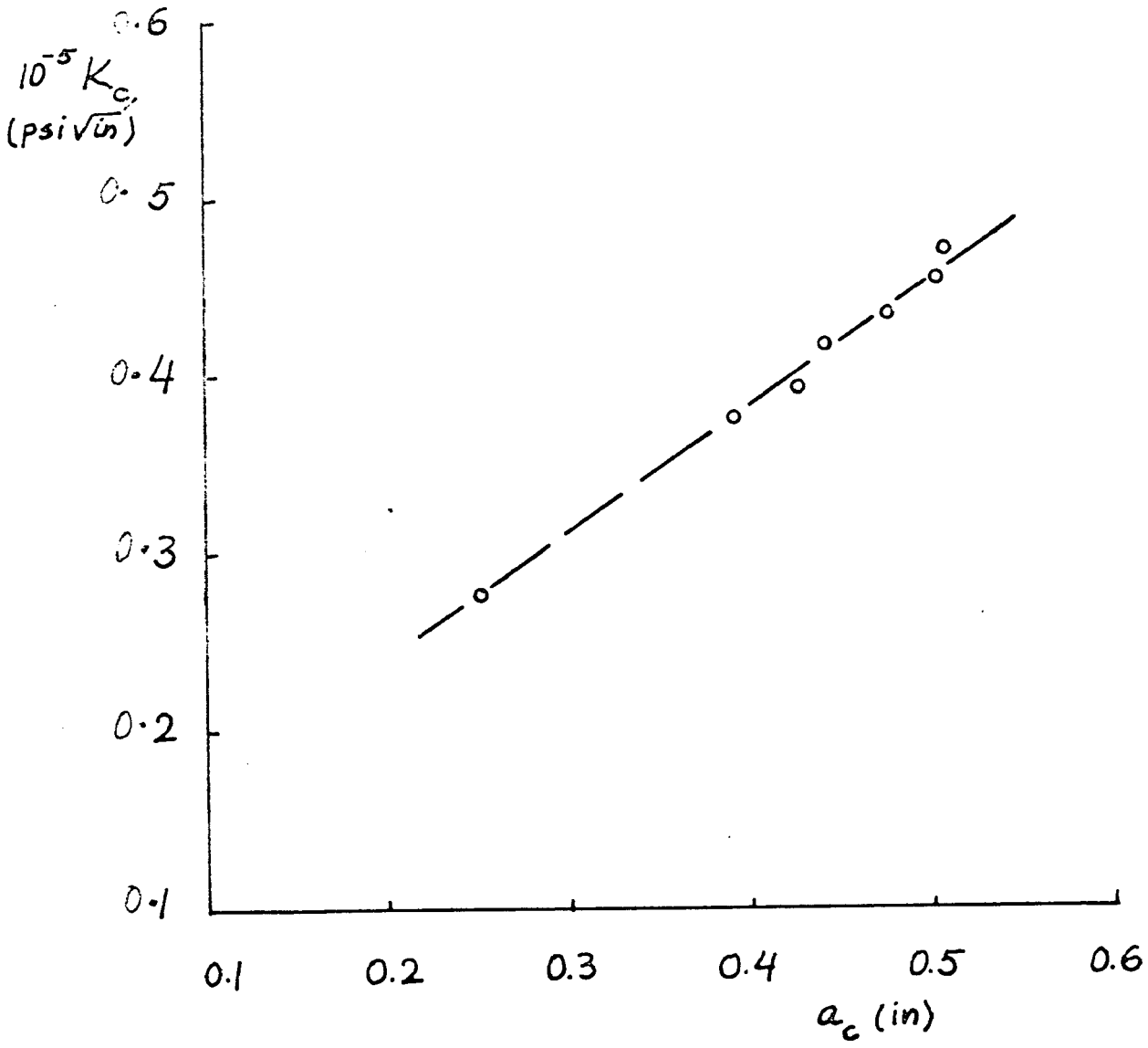

Figure 11. Stress intensity factor at the onset of rapid fracture vs. crack length in shells

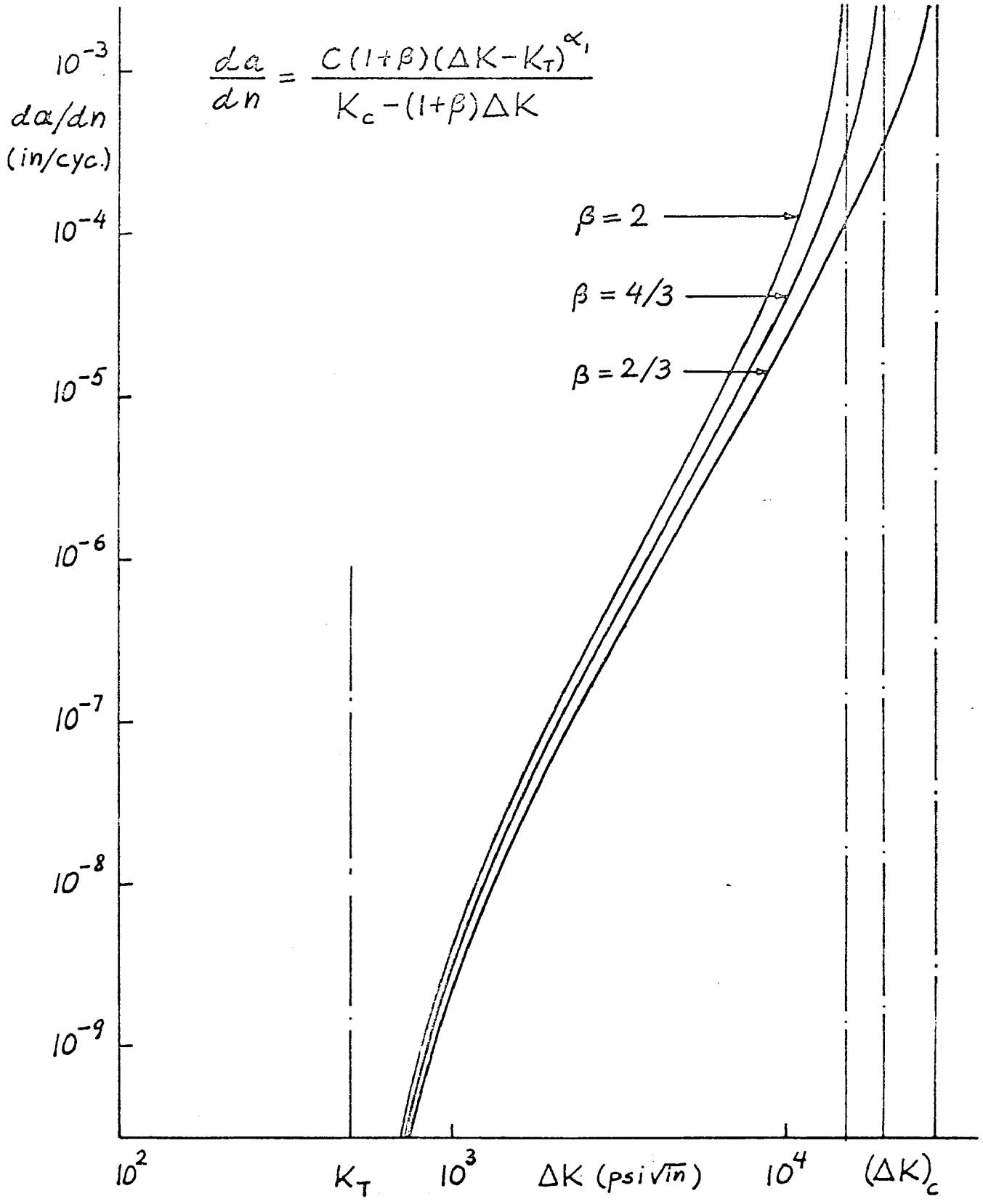

Figure 12. Fatigue crack propagation obtained from the model given by equation (5).

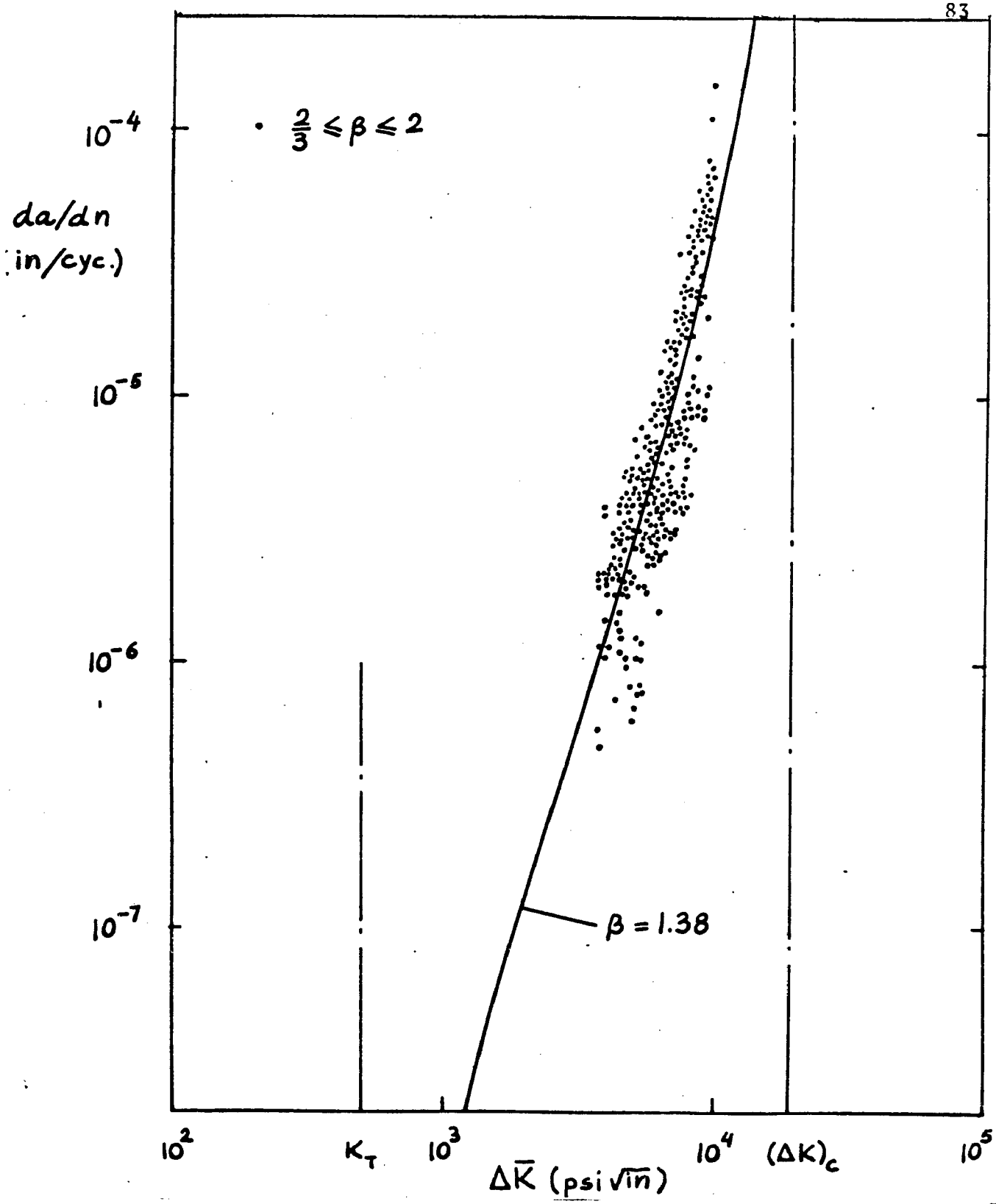

Figure 13. Combined fatigue data for shells. Solid curve is obtained from equation (5) by using an average load ratio, $\beta = 1.38$.

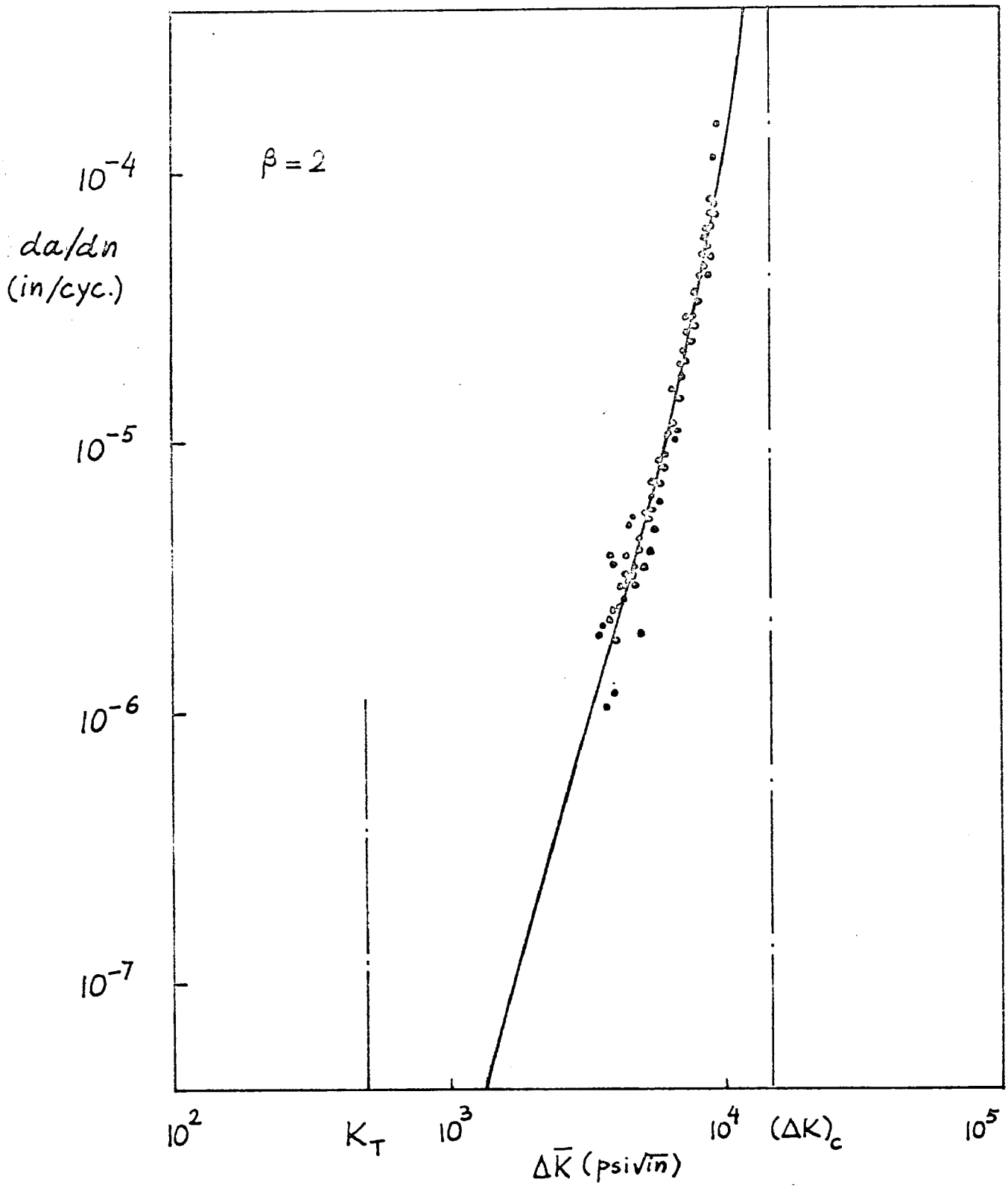

Figure 14. Crack growth rates in shells for β = 2. The solid curve is obtained from (5).

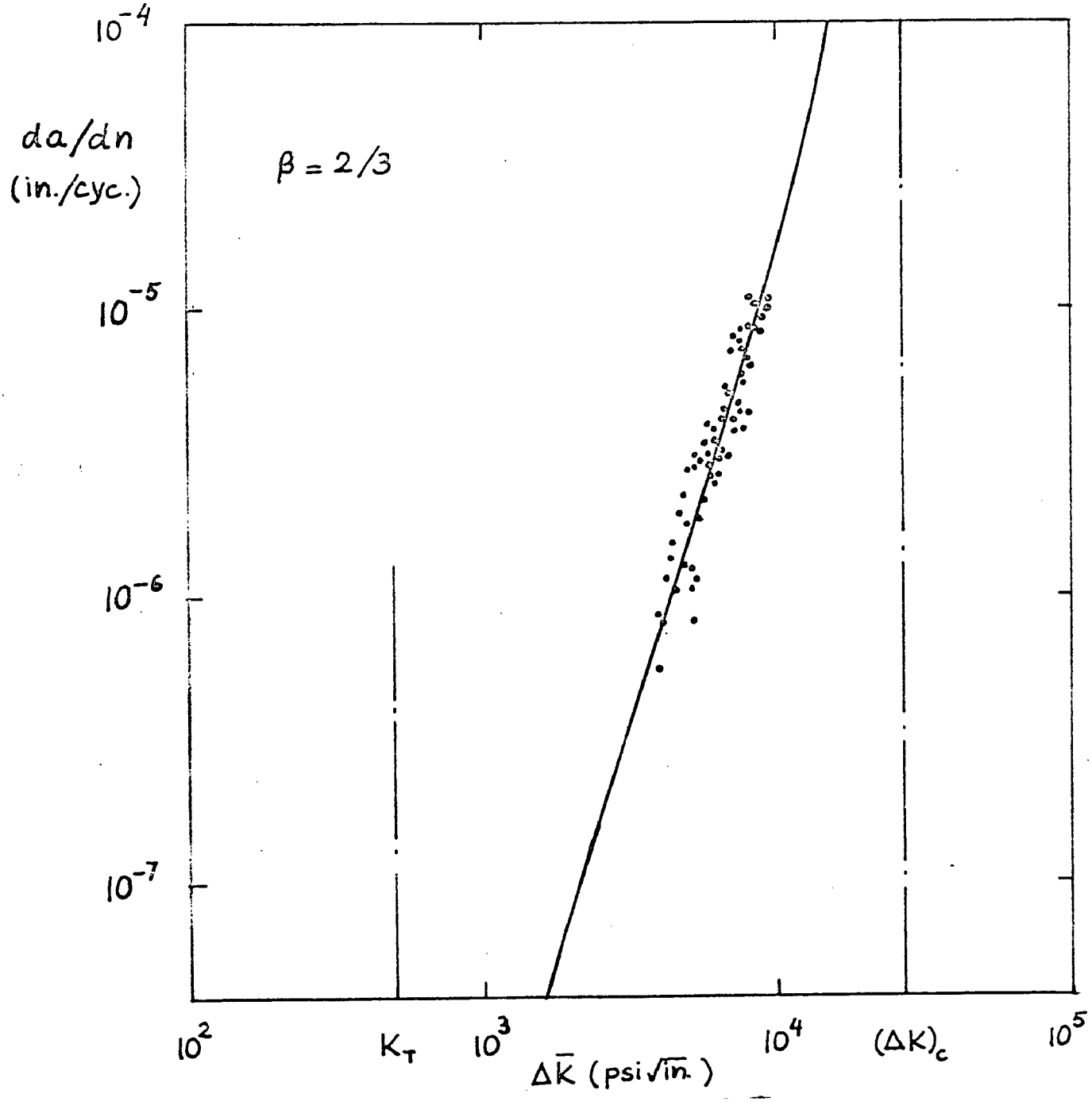

Figure 15. Crack growth rates in shells for $\beta = 2/3$. The solid curve is obtained from (5).

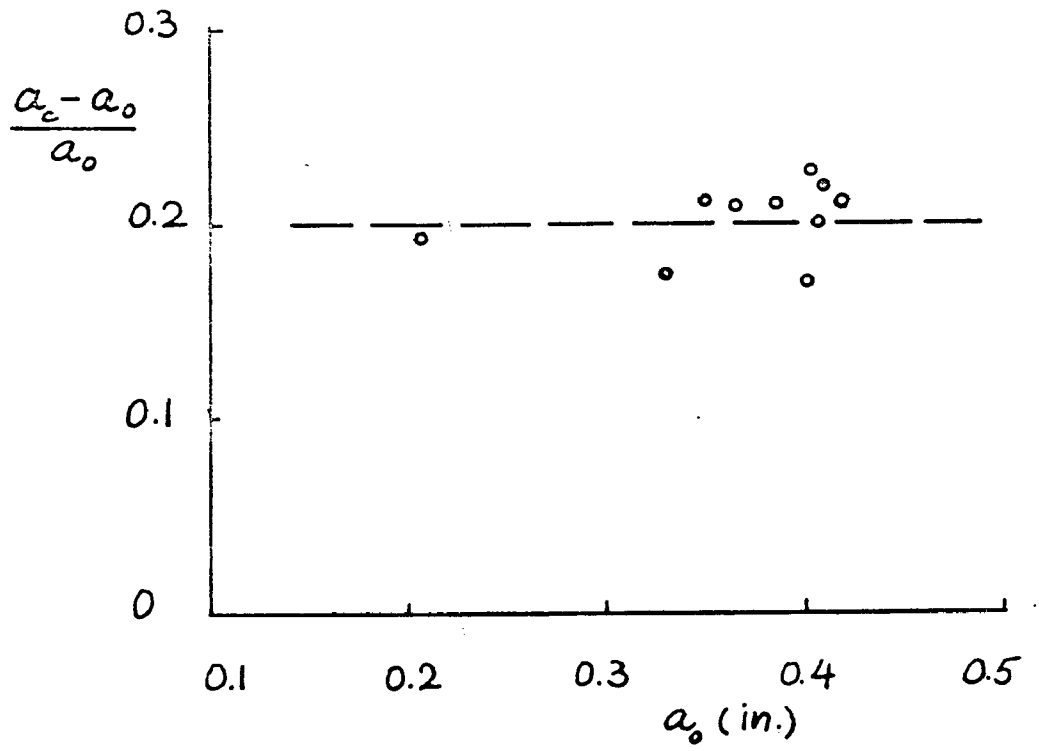

Figure 16. Slow crack extension vs. crack length in shells under slowly increasing axial tension

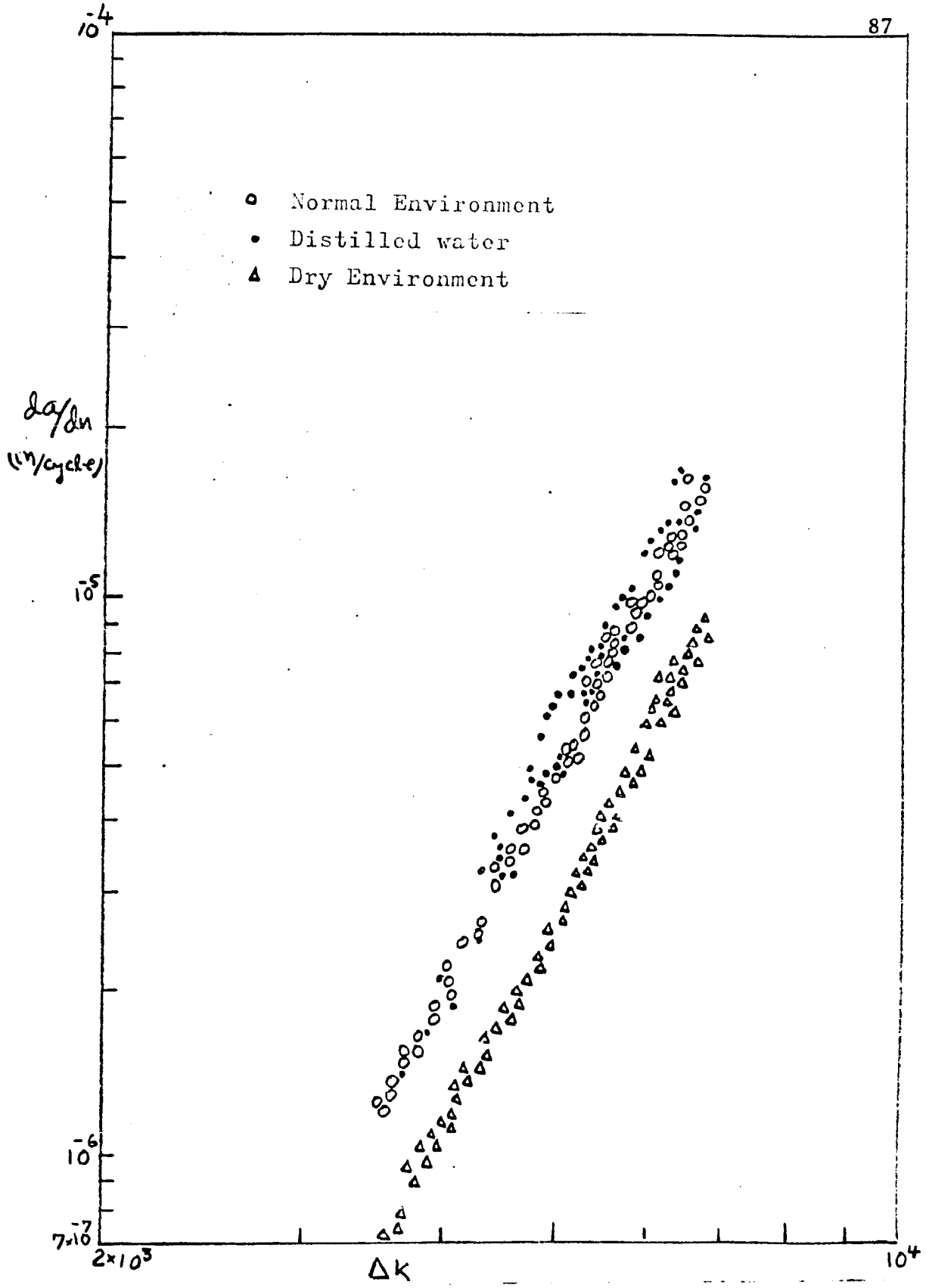

Figure 17. Crack growth rates in plates for β = 2.0 under various environments

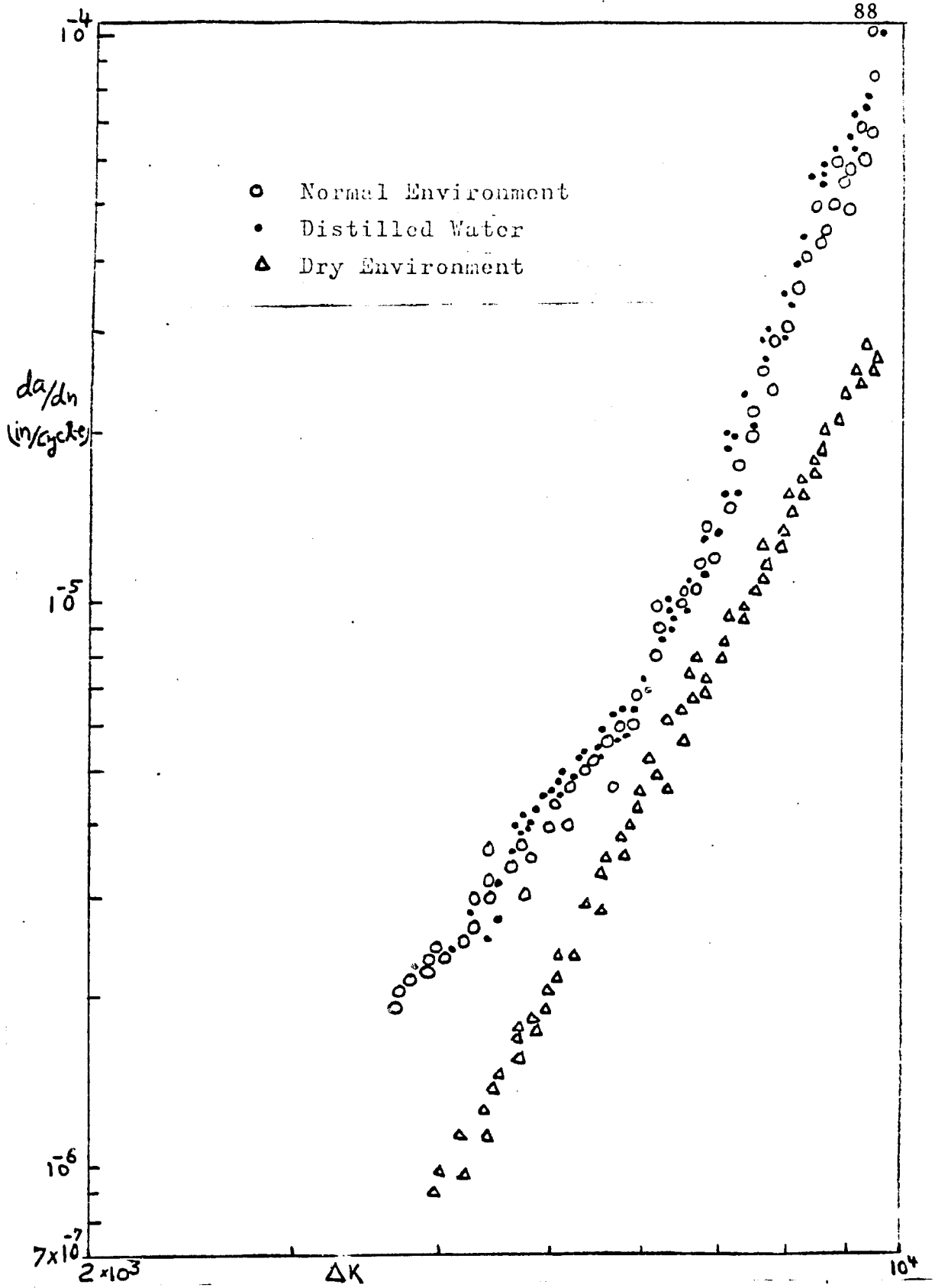

Figure 18. Crack growth rates in shells for β = 2.0 under various environments

TABLE I

6061-T4 Shell and Plate Specimens

Shells

Thickness:	$h = 0.022$ in.
Radius:	$R = 1.736$ in.
Free Length:	$2\ell = 12$ in.
0.2% offset yield, Axial direction:	$\sigma_y = 22{,}000$ psi
	$\sigma_{ult,} = 37{,}600$ psi
% Elongation:	15.8
Under uncontrolled environments	
Load Ratio:	$\beta = 0.67 - 2.0$
Number of Specimens:	13
Under controlled environments	
Load Ratio:	$\beta = 2$
Number of Specimens:	2 under each condition
Mean Stress:	12,000 psi

TABLE I

Plates

Thickness:	$h = 0.025$ in.
Width:	$2b = 6.5$ in.
Length:	$2\ell = 16$ in.
0.2% offset yield, perpendicular to rolling direction	$\sigma_y = 24{,}000$ psi
	$\sigma_{ult.} = 37{,}900$ psi
% Elongation:	15.1
Under uncontrolled environments	
Load Ratio:	$\beta = 1.05 - 3.50$
Number of Specimens:	25
Under controlled environments	
Load Ratio:	$\beta = 2$
Number of Specimens:	2 under each condition
Mean Stress:	12,000 psi

TABLE II

Stress Intensity Factor Ratios for Tension and Torsion

	Tension		Torsion	
λ	B_m	$10^3 \times B_b$	C_m	$10^6 \times C_b$
0	1.0	0	1.0	0
1	1.0439	1.9851	1.0440	1.5930
2	1.1496	2.6240	1.4960	2.9339
3	1.2847	2.6633	1.2847	1.1360
4	1.4290	1.6377	1.4291	0.3703
5	1.5715	-1.1083	1.5714	-0.1830
6	1.7069	-6.0770	1.7068	-0.4778
7	1.8339	-13.411	1.8338	-1.0644
8	1.9530	-22.870	1.9529	-1.1555
9	2.0657	-33.952		
10	2.1712	-46.062	2.1714	-1.4616

TABLE III

Material Parameters for 6061-T4 Obtained from Eq. (1)

Shell

m	α	10^{15} C (psi$\sqrt{in}$)	10^{15} C (α = 3.5)	S.E.
1	3.4016	11.29	4.790	0.432
1.5	3.394	7.616	3.036	0.424
2	3.387	5.136	1.921	0.429

Plate

m	α	10^{15} C (psi$\sqrt{in}$)	10^{15} C (α = 3.5)	S.E.
1	3.800	3.670	5.100	0.385
1.5	4.010	0.034	3.124	0.418
2	4.232	0.00313	1.914	0.48

TABLE IV

Material Parameters for 6061-T4 Obtained from Eq. (4.1)

σ_{mean} = 12,000 psi , β = 2.0

Shells

m	α	10^{15} C ($psi\sqrt{in}$)	10^{15} C (α = 3.5)	S.E.
Uncontrolled Environments				
1	3.3099	25.553	4.8702	0.282
1.5	3.3099	14.753	2.8118	0.282
2	3.3099	8.5177	1.6234	0.282
Hundred Per Cent Humidity				
1	3.8881	0.164	4.882	0.232
1.5	3.8881	0.09469	2.8189	0.232
2	3.8881	0.05467	1.627	0.232
Approximately Zero Per Cent Humidity				
1	3.2325	23.324	2.239	0.107
1.5	3.2325	13.466	1.293	0.107
2	3.2325	7.774	0.7465	0.107

TABLE IV

Plates

σ_{mean} = 12,000 psi , β = 2.0

m	α	10^{15} C (psi$\sqrt{in}$)	10^{15} C (α = 3.5)	S.E.
Uncontrolled Environments				
1	3.4932	5.7019	5.3828	0.0497
1.5	3.4932	3.2920	3.1077	0.0497
2	3.4932	1.9006	1.7942	0.0497
Hundred Per Cent Humidity				
1	3.5923	2.5799	5.704	0.337
1.5	3.5923	1.489	3.293	0.337
2	3.5923	0.8599	1.9015	0.337
Approximately Zero Per Cent Humidity				
1	3.623	1.0279	2,944	0.122
1.5	3.623	0.5934	1.700	0.122
2	3.623	0.3426	0.981	0.122

APPENDIXES

APPENDIX I

Anti-Symmetric Problem

The kernels h_{ij} and k_{ij} are

$$h_{11}(t,y) = \lim_{x\to 0} \int_0^\infty \left[s_1^{-1} e^{-s_1|x|} + s_2^{-1} e^{-s_2|x|} \right] s \sin\{s(t-y)\}\, ds.$$

$$h_{12}(t,y) = \lim_{x\to 0} \int_0^\infty \left[-\left(\frac{s}{s_1} + \frac{\alpha_1^2}{s s_1}\right) e^{-s_1|x|} + \left(\frac{\nu s}{s_2} + \frac{\alpha_2^2}{s s_2}\right) e^{-s_2|x|} \right] \sin\{s(t-y)\}\, ds.$$

$$h_{21}(t,y) = \lim_{x\to 0} \int_0^\infty \left[\left\{ \frac{4\alpha_1^2}{s_1} + (1+\nu)\frac{s^2}{s_1} \right\} e^{-s_1|x|} - \left\{ \frac{4\alpha_2^2}{s_2} + (1+\nu)\frac{s^2}{s_2} \right\} e^{-s_2|x|} \right] \left[\sin st - \sin s(t-y) \right] \frac{ds}{s}$$

$$h_{22}(t,y) = \lim_{x\to 0} \int_0^\infty \left[\left\{ -\frac{4\alpha_1^2 s_1}{s^2} + (1-\nu)s_1 \right\} e^{-s_1|x|} + \left\{ -\frac{4\alpha_2^2 s_2}{s^2} + (1-\nu)\left(s_2 + \frac{4\alpha_2^2}{s_2}\right) + (1-\nu^2)\frac{s^2}{s_2} \right\} e^{-s_2|x|} \right] \left[\sin st - \sin s(t-y) \right] ds/s.$$

$$k_{11}(t,y) = \int_0^\infty \left(\frac{s}{s_1} + \frac{s}{s_2} - 2 \right) \sin\{s(t-y)\}\, ds.$$

$$K_{12}(t,y) = \int_0^\infty ds\left(-\frac{s}{S_1} + 1 + \nu\frac{s}{S_2} - \nu - \frac{\alpha_1^2}{sS_1} + \frac{\alpha_2^2}{sS_2}\right)\sin s(t-y)$$

$$K_{22}(t,y) = \int_0^\infty \left[(1-\nu)\frac{s}{S_1} + (2-\nu-\nu^2)\frac{s}{S_2} - (1-\nu)(3+\nu) - \frac{3+\nu}{sS_1}\alpha_1^2\right.$$

$$\left. + \frac{(1-5\nu)\alpha_2^2}{sS_2}\right]\left[\sin st - \sin\{s(t-y)\}\right] ds - 4\int_0^\infty \left[\frac{\alpha_1^4}{S_1 s^3}\right.$$

$$\left. + \frac{\alpha_2^4}{S_2 s^3}\right]\left(1-\cos(sy)\right)\sin(st) + \frac{(1-\nu)(3+\nu)}{t}$$

$$k_{21}(t,y) = \int_0^\infty \left[\frac{4\alpha_1^2}{sS_1} - \frac{4\alpha_2^2}{sS_2} + (1+\nu)\left(\frac{s}{S_1} - \frac{s}{S_2}\right)\right]$$

$$\left[\sin(st) - \sin\{s(t-y)\}\right] ds.$$

Defining

$$s^2 + \alpha_1^2 = R e^{i\varphi}$$

$$s^2 + \alpha_2^2 = R e^{-i\varphi}$$

$$S_1 = R^{1/2} e^{i\varphi/2}$$

$$S_2 = R^{1/2} e^{-i\varphi/2}$$

where $R^2 = s^4 + \left(\frac{\lambda}{2}\right)^4$

$$\varphi = \tan^{-1}\left[\frac{(\lambda/2)^2}{s^2}\right]$$

$$\cos\frac{\varphi}{2} = \frac{(\lambda/2)^2}{2^{1/2}\left[(\lambda/2)^4 + s^4 - s^2\left\{s^4 + (\lambda/2)^4\right\}^{1/2}\right]^{1/2}}$$

$$\sin\frac{\varphi}{2} = \frac{\left[(\lambda/2)^4 + s^4\right]^{1/2} - s^2}{2^{1/2}\left[\left(\frac{\lambda}{2}\right)^4 + s^4 - s^2\left\{s^4 + (\lambda/2)^4\right\}^{1/2}\right]^{1/2}}$$

The kernels can be written as

$$k_{11}(t,y) = 2\int_0^\infty \left[\frac{s}{R^{1/2}}\cos\frac{\varphi}{2} - 1\right]\sin\{s(t-y)\}\,ds$$

$$k_{12}(t,y) = -(1-\nu)\int_0^\infty \left[\frac{s}{R^{1/2}}\cos\frac{\varphi}{2} - 1\right]\sin\{s(t-y)\}\,ds$$

$$+ i(1+\nu)\int_0^\infty \frac{s}{R^{1/2}}\sin\frac{\varphi}{2}\sin\{s(t-y)\}\,ds$$

$$- i\lambda^2/2\int_0^\infty \frac{1}{sR^{1/2}}\cos\frac{\varphi}{2}\sin\{s(t-y)\}\,ds.$$

$$k_{21}(t,y) = i\,2(1+\nu)\int_0^\infty \frac{s}{R^{1/2}}\sin\frac{\varphi}{2}\sin\{s(t-y)\}\,ds$$

$$-i\,2\lambda^2\int_0^\infty s^{-1}R^{-1/2}\cos\frac{\varphi}{2}\sin\{s(t-y)\}\,ds$$

$$+i\,2(1+\nu)\int_0^\infty \frac{s}{R^{1/2}}\sin\frac{\varphi}{2}\sin(st)\,ds$$

$$- i\,2\lambda^2\int_0^\infty s^{-1}R^{-1/2}\cos\frac{\varphi}{2}\sin(st)\,ds.$$

$$K_{22}(t,y) = -(1+\nu)(3+\nu)\int_0^\infty \left[\frac{s}{R^{1/2}}\cos\frac{\varphi}{2} - 1\right]\sin\{s(t-y)\}\,ds$$

$$- i(1-\nu^2)\int_0^\infty \frac{s}{R^{1/2}}\sin\frac{\varphi}{2}\sin\{s(t-y)\}\,ds.$$

$$+ i(1-\nu)\lambda^2\int_0^\infty \frac{\cos\varphi/2}{sR^{1/2}}\sin\{s(t-y)\}\,ds$$

$$+ \frac{1+3\nu}{2}\int_0^\infty \frac{\sin\varphi/2}{sR^{1/2}}\sin\{s(t-y)\}\,ds$$

$$+ \frac{\lambda^4}{2}\int_0^\infty \frac{\cos\varphi/2}{s^3R^{1/2}}(\cos(ys)-1)\sin(st)\,ds$$

$$- (1-\nu)(3+\nu)\int_0^\infty \left[\frac{s}{R^{1/2}}\cos\varphi/2 - 1\right]\sin\{s(t-y)\}\,ds$$

$$- i(1-\nu^2)\int_0^\infty \frac{s}{R^{1/2}}\sin\frac{\varphi}{2}\sin(st)\,ds$$

$$+ i(1-\nu)\lambda^2\int_0^\infty \frac{\cos\varphi/2}{sR^{1/2}}\sin\{s(t-y)\}\,ds.$$

$$+ (1+3\nu)2^{-1}\int_0^\infty \frac{\sin\varphi/2}{sR^{1/2}}\sin(st)\,ds$$

APPENDIX II

Symmetric Problem

The functions w and F are defined as

$$w(x,y) = \int_0^\infty \Big[Q_1 e^{(\alpha_1 - s_1)|x|} + Q_2 e^{-(\alpha_1 + s_1)|x|} + Q_3 e^{-(\alpha_2 + s_2)|x|} + Q_4 e^{(\alpha_2 - s_2)|x|} \Big] \cos(sy)\, ds.$$

$$F(x,y) = \frac{iEha^2}{\lambda^2 R} \int_0^\infty \Big[Q_1 e^{(\alpha_1 - s_1)|x|} + Q_2 e^{-(\alpha_1 + s_1)|x|} - Q_3 e^{-(\alpha_2 + s_2)|x|} - Q_4 e^{(\alpha_2 - s_2)|x|} \Big] \cos(sy)\, ds$$

Two relations between Q_j are found from the conditions

$$V_x(0,y) = 0$$

and $$N_{xy}(0,y) = 0, \qquad y \geq 0$$

The relations between Q_j are given by

$$Q_3 - Q_4 = \nu \frac{\alpha_1}{\alpha_2} (Q_1 - Q_2) + \nu_0 \frac{s_1}{\alpha_2} (Q_1 + Q_2)$$

$$Q_3 + Q_4 = -(1 + \nu) \frac{\alpha_1}{s_2} (Q_1 - Q_2) + \nu \frac{s_1}{s_2} (Q_1 + Q_2)$$

Two more relations for Q_j are obtained in the form of a system of integral equations by using the following boundary conditions at x = 0.

$$M_x(0,y) = -\frac{D}{a^2}\left[\frac{\partial^2 W}{\partial x^2} + \nu \frac{\partial^2 W}{\partial y^2}\right] = \frac{D m_0}{a^2}$$

$$N_x(0,y) = \frac{1}{a^2}\frac{\partial^2 F}{\partial y^2} = \frac{n_0}{a^2}$$

The continuity conditions on the functions and their derivatives for x = 0 and $|y| > 1$ are satisfied if

$$\int_0^\infty s_1 (Q_1 + Q_2) \cos(sy)\, ds = 0$$

$$\int_0^\infty \alpha_1 (Q_1 - Q_2) \cos(sy)\, ds = 0$$

The functions φ_i (i = 1,2) are defined as

$$\int_0^\infty s_1 (Q_1 + Q_2) \cos(sy)\, ds = \begin{cases} \varphi_1(y) & |y| < 1 \\ 0 & |y| > 1 \end{cases}$$

$$\int_0^\infty \alpha_1 (Q_1 - Q_2) \cos(sy)\, ds = \begin{cases} \varphi_2(y) & |y| < 1 \\ 0 & |y| > 1 \end{cases}$$

With the above definition of φ_1 and φ_2 the symmetric problem is reduced to the solution of a set of integral equations given by (2.35).

The kernels are given by

$$L_{11}(y,t) = \lim_{|x|\to 0} \int_0^\infty \left[\frac{s e^{-s_1|x|}}{s_1} - \nu \frac{s e^{-s_2|x|}}{s_2}\right] \sin\{(t-y)s\}\, ds$$

$$L_{12}(y,t) = \lim_{|x|\to 0} (1+\nu) \int_0^\infty \frac{s e^{-s_2|x|}}{s_2} \sin\{s(t-y)\}\, ds$$

$$L_{21}(y,t) = \lim_{|x|\to 0} \int_0^\infty \left[(1-\nu)\frac{s e^{-s_1|x|}}{s_1} + (2+\nu)(1-\nu)\frac{s e^{-s_2|x|}}{s_2}\right] \sin\{s(t-y)\}\, ds + \frac{i\lambda^2}{2}\int_0^\infty \left(\frac{1}{s s_1} - \frac{1}{s s_2}\right) \sin\{s(t-y)\}\, ds$$

$$L_{22}(y,t) = \lim_{|x|\to 0} -\int_0^\infty \left[\frac{2 s e^{-s_1|x|}}{s_1} + (1-2\nu-\nu^2)\frac{s e^{-s_2|x|}}{s_2}\right] \sin\{s(t-y)\}\, ds - \frac{i\lambda^2}{2}\int_0^\infty \left(\frac{1}{s s_1} - \frac{1}{s s_2}\right) \sin\{s(t-y)\}\, ds$$

$$R_{11}(y,t) = \int_0^\infty \left(\frac{s}{s_1} - 1\right) \sin\{s(t-y)\}\, ds - \nu \int_0^\infty \left(\frac{s}{s_2} - 1\right) \sin\{s(t-y)\}\, ds$$

$$R_{12}(y,t) = (1+\nu) \int_0^\infty \left(\frac{s}{s_2} - 1\right) \sin\{s(t-y)\}\, ds.$$

$$R_{21}(y,t) = (1-\nu)\int_0^\infty \left(\frac{s}{s_1}-1\right) \sin\{s(t-y)\}\,ds$$

$$+(2+\nu)(1-\nu)\int_0^\infty \left(\frac{s}{s_2}-1\right) \sin\{s(t-y)\}\,ds$$

$$+\frac{i\lambda^2}{2}\int_0^\infty \left(\frac{1}{ss_1}-\frac{1}{ss_2}\right) \sin\{s(t-y)\}\,ds$$

$$R_{22}(y,t) = -2\int_0^\infty \left(\frac{s}{s_1}-1\right) \sin\{s(t-y)\}\,ds$$

$$-(1-2\nu-\nu^2)\int_0^\infty \left(\frac{s}{s_2}-1\right) \sin\{s(t-y)\}\,ds$$

$$-\frac{i\lambda^2}{2}\int_0^\infty \left(\frac{1}{ss_1}-\frac{1}{ss_2}\right) \sin\{s(t-y)\}\,ds$$

Separating the real and imaginary parts of the kernels, the kernels can be written as

$$R_{11}(t,y) = (1-\nu)\int_0^\infty \left[\frac{s}{R^{1/2}}\cos\frac{\varphi}{2}-1\right] \sin\{s(t-y)\}\,ds$$

$$-i(1+\nu)\int_0^\infty \frac{s}{R^{1/2}} \sin\frac{\varphi}{2} \sin\{s(t-y)\}\,ds$$

$$R_{12}(t,y) = (1+\nu)\int_0^\infty \left[\frac{s}{R^{1/2}}\cos\frac{\varphi}{2}-1\right] \sin\{s(t-y)\}\,ds$$

$$+i(1+\nu)\int_0^\infty \frac{s}{R^{1/2}} \sin\frac{\varphi}{2} \sin\{s(t-y)\}\,ds$$

$$R_{21}(t,y) = (3+\nu)(1-\nu)\int_0^\infty \left[\frac{S}{R^{1/2}}\cos\frac{\varphi}{2} - 1\right]\sin\{s(t-y)\}\,ds$$

$$+ i(1-\nu^2)\int_0^\infty \frac{S}{R^{1/2}}\sin\frac{\varphi}{2}\sin\{s(t-y)\}\,ds$$

$$+ \lambda^2\int_0^\infty \frac{\sin\varphi/2}{sR^{1/2}}\sin\{s(t-y)\}\,ds$$

$$R_{22}(t,y) = -(3+\nu)(1-\nu)\int_0^\infty \left[\frac{S}{R^{1/2}}\cos\frac{\varphi}{2} - 1\right]\cdot$$

$$\cdot\sin\{s(t-y)\}\,ds$$

$$- \lambda^2\int_0^\infty \frac{\sin\frac{\varphi}{2}}{sR^{1/2}}\sin\{s(t-y)\}\,ds$$

$$- i(1+\nu)^2\int_0^\infty \frac{S}{R^{1/2}}\sin\frac{\varphi}{2}\sin\{s(t-y)\}\,ds$$

APPENDIX III

As discussed in Chapter II, the solution of the problem for symmetrically loaded shell with a circumferential crack is reduced to

$$\int_{-1}^{+1} \sum_{1}^{2} a_{ij}\, \varphi_j(t) \frac{dt}{t-y} + \int_{-1}^{2} \sum_{1}^{2} R_{ij}\, \varphi_j(t)\, dt = f_j(y)$$

$$i = 1, 2.$$

where the coefficients a_{ij} and kernels R_{ij} for symmetric loading are given earlier. The functions $f_j(y)$ are given in terms of crack surface tractions as

$$f_1(y) = \frac{\pi \lambda^2 R}{i E h} \int_0^y N_x(y)\, dy.$$

$$f_2(y) = \frac{\pi a^2}{D} \int_0^y M_x(y)\, dy$$

In the calculations of the plastic zone size, the stress intensity factor ratios $A_m(\lambda_p)$ and $A_b(\lambda_p)$ shown in equation (3.2) are obtained by letting $N_y = -N_o$ and $M_y = 0$ and are obtained in symmetric problem. For the calculation of B_{ij} shown in (3.4) the tractions are given

by (3.3). Thus the input functions become

$$f_1(y) = \begin{cases} 0 & |y| < \alpha \\ \dfrac{\pi \lambda_p^2 R}{i E h} N(y-\alpha) , & \alpha < |y| < 1 \end{cases}$$

$$f_2(y) = \begin{cases} 0 & |y| < \alpha \\ \dfrac{\pi a^2}{D} M(y-\alpha) , & \alpha < |y| < 1 \end{cases}$$

However, in the case under consideration the effect of bending is neglected and hence $f_2(y) = 0$.

REFERENCES

REFERENCES

[1] E. S. Folias, "A finite line crack in a pressurized spherical shell," Int. J. Fracture Mechanics, Vol. 1, p. 20 (1965).

[2] E. S. Folias, "An axial crack in a pressurized cylindrical shell," Ibid., Vol. 1, p. 104 (1965).

[3] E. S. Folias, "A circumferential crack in a pressurized cylinder," Ibid., Vol. 3, p. 1 (1967).

[4] L. G. Copley and J. L. Sanders, Jr., "A longitudinal crack in a cylindrical shell under internal pressure," Ibid., Vol. 5, p. 117 (1969).

[5] M. E. Duncan and J. L. Sanders, Jr., "The effect of circumferential stiffener on the stress in a pressurized cylindrical shell with a longitudinal crack," Ibid., Vol. 5, p. 133 (1969).

[6] F. Erdogan and J. J. Kibler, "Cylindrical and spherical shells with cracks, " Ibid., Vol. 5, p. 229 (1969).

[7] G. R. Irwin, "Plastic zone near a crack and fracture toughness," Proc. Sagamore Res. Ord. Materials, p. 63 (1960).

[8] A. A. Wells, "Notched bar tests, fracture mechanics and the brittle strengths of welded structures," B.W.J. Vol. 12, p. 2 (1962).

[9] D. S. Dugdale, "Yielding of steel sheets containing slits," J. Mech. Phys. Solids Vol. 8, p. 100 (1960).

[10] G. I. Barenblatt, "Mathematical theory of equilibrium cracks in brittle fracture," Advances in Applied Mechanics, Vol. 7, p. 55 (1962).

[11] B. A. Bilby, A. H. Cottrell and K. H. Swinden, "The spread of plastic yielding from a notch," Proc. Roy. Soc. A 272 p. 304 (1963).

[12] B. A. Bilby, A. H. Cottrell, E. Smith and K. H. Swinden, "Plastic yielding from sharp notches," Proc. Roy. Soc. A 279, p. 1 (1964).

[13] F. Erdogan, "Elastic-plastic anti-plane problems for bonded dissimilar media containing cracks and cavities," Int. J. Solids and Struct., Vol. 2, p. 447 (1966).

[14] K. Marguerre, "Zur Theorie der Gekrummten Platte grosser Formanderung," Proc. 5 Int. Cong. Appl. Mech. p. 93 (1938).

[15] N. I. Muskhlishville, "Singular Integral Equations," P. Noordhoff Gronigen (1953).

[16] F. Erdogan, "Approximate solutions of system of singular integral equations," SIAM J. Appl. Math., Vol. 7, p. 1041 (1969).

[17] Abramowitz and Stegun, T. A., Editors, "Handbook of Mathematical Functions," National Bureau of Standards, Appl. Math. Series 55, 1964, p. 384.

[18] F. Erdogan, "Crack propagation theories," Fracture, An Advanced Treatise, Edited by H. Liebowitz, Vol. 2, Chapter 5, Academic Press, 1968.

[19] R. G. Forman, V. E. Kearney and R. M. Emgle, "Numerical analysis of cyclic loaded structures," J. Basic Engineering, Trans. ASME, Vol. 89, Series D, p. 459, 1967.

[20] G. T. Hahn, M. Sarrate and A. R. Rosenfield, "Criteria for crack extension in cylindrical pressure vessels," Int. J. Fracture Mechanics, Vol. 5, p. 187, 1969.

[21] "Fracture Testing of High-Strength Sheet Materials," First report, ASTM Committee on Fracture Testing of High Strength Sheet Materials, ASTM Bulletin 243, p. 29, Jan. 1960.

[22] J. C. Newman, Jr., "Fracture of cracked plates under plane stress," Engineering Fracture Mechanics, Vol. 1, p. 137, 1968.

[23] P. C. Paris and R. A. Schmidt, The Laboratory Staff of Del Research Corporation, and W. L. Weiss, "Very slow fatigue crack growth rates in a steel alloy," National Symposium on Fracture Mechanics, August 1969, Bethlehem, Pa.

[24] J. J. Kibler, "A study of fatigue and fracture of plates and shells," Ph.D. Thesis, Lehigh University, Bethlehem, Pa., 1969.

[25] N. N. Wang, "Effects of plate thickness in the bending of an elastic plate containing a crack," J. Math. Phys., Vol. 48, p. 371, 1969.

[26] A. Hartman, "On the effect of oxygen and water vapor on the propagation of fatigue cracks in 2024-T3 Alclad Sheet," Int. J. Fract. Mech. 1, 167 (1965).

[27] F. J. Bradshaw and C. Wheeler, "The effect of environment on fatigue crack growth in aluminum and some aluminum alloys," Appl. Mater. Res. 5, 112 (1966).

[28] R. P. Wei, "Fatigue crack propagation in high strength aluminum alloys," Int. J. Fract. Mech. 4, 159 (1968).

[29] R. P. Wei, "Some aspects of environmental enhanced fatigue crack growth," Engineering Fracture Mechanics, Vol. 1, 1970.

[30] F. Erdogan and M. Ratwani, "Plasticity and the crack opening displacement in shells," NASA Report, Dept. of M.E. and Mech., Lehigh University, Bethlehem, Pa., April 1970.

[31] R. B. Anderson and T. L. Sullivan, "Fracture mechanics of through cracked cylindrical pressure vessels," NASA TND-3252 (1966).

VITA

Mohan Ratwani, son of Mr. and Mrs. Menghraj Ratwani, was born on May 15, 1939 in Hyderabad, India. He attended public primary and secondary schools in Ajmer, India. In June 1956, he entered Baroda University in India and received the degree of Bachelor of Engineering in June 1959.

He received a Government of India Fellowship and entered the graduate school at Poona University, India, in August 1960, and received the degree of Master of Science in Civil Engineering in June 1962.

He worked as a lecturer in Delhi College of Engineering, Delhi, from August 1962 to May 1966 and as a lecturer in Indian Institute of Technology, Delhi, from June 1966 to August 1967.

He joined Lehigh University as a graduate student in September 1967. While at Lehigh University he has had the opportunity to present some of his research findings as co-author in the papers:

> F. Erdogan and M. Ratwani, "Fatigue and fracture of cylindrical shells containing circumferential cracks," to be published in International Journal of Fracture Mechanics, 1970.

F. Erdogan and M. Ratwani, "Plasticity and the crack opening displacement in shells," NASA Report, Dept. of M.E. & Mech., Lehigh University, Bethlehem, Pa. (April 1970).

F. Erdogan and M. Ratwani, "A circumferential crack in a cylindrical shell under torsion," NASA Report, Dept. of M.E. & Mech., Lehigh University, Bethlehem, Pa. (June 1970).